HOKKAIDO UNIVERSITY

Title	Li-N-H System for Hydrogen Storage: An Investigation on Reaction Mechanism and Catalytic Effect
Author(s)	張, 騰飛
Degree Grantor	北海道大学
Degree Name	博士(工学)
Dissertation Number	甲第11880号
Issue Date	2015-03-25
DOI	https://doi.org/10.14943/doctoral.k11880
Doc URL	https://hdl.handle.net/2115/60909
Type	doctoral thesis
File Information	Zhang_Tengfei.pdf

Hokkaido University Collection of Scholarly and Academic Papers : HUSCAP

Li-N-H System for Hydrogen Storage: An Investigation on Reaction Mechanism and Catalytic Effect

By

Tengfei ZHANG

A thesis submitted in fulfillment of the requirements for the degree of Philosophiae Doctor (PhD)

Examination Committee: Prof. Somei OHNUKI
Prof. Shigeharu UKAI
Prof. Tomohiro AKIYAMA
Prof. Naoyuki HASHIMOTO

PhD Thesis No. EG-
Division of Materials Science and Engineering
Graduate School of Engineering, Hokkaido University
March 2015

‘昨夜西风凋碧树，独上高楼，望尽天涯路。’

晏殊《蝶恋花》

‘衣带渐宽终不悔，为伊消得人憔悴。’

柳永《蝶恋花》

‘众里寻他千百度，暮然回首，那人却在，灯火阑珊处。’

辛弃疾《青玉案》

《诗经-卫风-淇奥》

瞻彼淇奥，绿竹猗猗。

有匪君子，如切如磋，如琢如磨。

瑟兮僩兮，赫兮喧兮，

有匪君子，终不可谖兮！

瞻彼淇奥，绿竹青青。

有匪君子，充耳琇莹，会弁如星。

瑟兮僩兮，赫兮喧兮，

有匪君子，终不可谖兮！

瞻彼淇奥，绿竹如箦。

有匪君子，如金如锡，如圭如璧。

宽兮绰兮，猗重较兮，

善戏谑兮，不为虐兮！

Abstract

Hydrogen is a kind of independent carrier in comparison to conventional ones, including fossil fuels. It accompanies following advantages such as clean, environmental friendliness and forming water as a non-polluting product during practical applications. Accordingly, reductions of dependence on fossil fuels and emissions of pollutants and greenhouse gases could be realized after using hydrogen as a primary fuel successfully.

Lithium-nitrogen-hydrogen system has been well studied as hydrogen storage materials, since its relatively high capacity of hydrogen and good reversibility during de/hydrogenation. Furthermore, the cost of starting materials is lower than fossil fuels. However, there still have some parts not clearly in this system. Firstly, the reaction mechanism in nano scale between lithium hydride and lithium amide is still need to be investigated in details. To date, little evidence could be acquired from the recent literature showing the position and phase change between each solid phase. Moreover, previous research has shown that some catalysts, especially titanium compounds, have an effect on improving both the hydrogen absorption and desorption kinetics of this system. However, the catalysts which are effective for the de/hydrogenation in the nano scale have not yet been clearly understood. Last but not least, according to the previous approach, from the standpoint of the tuning of small ion mobility, one attempt to enhance the hydrogen-storage properties of the Li-N-H system is to target a catalyst that

would effectively increase the mobility of the Li^+ ions.

In the following chapters, these targets will be studied on the basis of a series of experiments. The conclusion will be carefully shown after discussions.

In Chapter 2, it covers the experimental techniques and equipment used during this study, a description of the material and its condition as well as the experimental procedures including details about the sample preparations for each technique. A variety of characterization equipment were used, including a pressure-composition-isotherm (PCI) device, a X-ray diffraction (XRD), two kinds of transmission electron microscope (TEM),a X-ray photoelectron spectroscopy (XPS), a alternating current (AC) impedance, a Thermo-gravimetry (TG), a differential thermal analysis (DTA) equipment and thermal gas desorption mass spectrometry (TDMS).

In Chapter 3, the decomposition mechanism of Li-N-H materials and the catalytic effect of Ti compounds in nano scale were investigated. LiH formed at the surface of $LiNH_2$ after hydrogenation. During dehydrogenation, LiH particles became smaller since it reacted with $LiNH_2$ at the interface. Ti compounds, $TiCl_3$ and $LiTi_2O_4$, located at the interface between LiH and $LiNH_2$. The decomposition mechanism and catalysis are believed to be: (a) Li^+ ion in LiH moved to $LiNH_2$ through the interface during dehydrogenation. At the same time, H combined and released at the interface; (b) the catalyst of Ti compounds is active in the interface between LiH and $LiNH_2$. It improves Li^+ ion migrate among LiH and $LiNH_2$/Li_2NH using less energy and improve the

desorption kinetics.

In Chapter 4, catalytic effects on the dehydrogenation properties of the Li-N-H system with $LiTi_2O_4$ additive were investigated. The appropriate amount and stability of $LiTi_2O_4$ on the system were confirmed by the results of TG-DTA-TDMS, XRD and XPS. During dehydrogenation, a storage capacity of 5.7 wt. % was obtained under moderate temperature. A sharp peak of hydrogen desorption occurred at 227 °C. $LiTi_2O_4$ is stable after high energy ball-milling and dehydrogenation which is reflected by the XRD patterns and XPS spectrums. The appropriate amount of additive is 0.5 mol % in the sample. The catalytic effect of $LiTi_2O_4$ probably results from the increasing of the Li^+ ions mobility between LiH and $LiNH_2$ solid phases.

In Chapter5, we have reported the discovery of the relationship between the catalytic effects and the lithium ionic mobility. The conductivity of $LiNH_2$ and LiH mixtures with catalyst is nearly 1.5 times higher than the sample without catalyst. The catalytic effects of $LiTi_2O_4$ probably results from enhancing the mobility of the Li^+ ions between the LiH and $LiNH_2$ solid phases. We note that the structure characters of $LiTi_2O_4$ could improve the Li^+ ionic conductivity which is beneficial to enhance the reaction kinetics. It is hoped that Li-N-H system could be used not only in hydrogen storage but also could be applied in the lithium-ion battery materials.

Chapter 6 is the conclusions of the whole work. Further discussion has been given.

CONTENTS

ABSTRACT V

CHAPTER 1 1

INTRODUCTION 1

1.1 HYDROGEN STORAGE BACKGROUND 3

1.2 COMPRESSED HYDROGEN 5

1.3 LIQUEFIED HYDROGEN 6

1.4 CHEMICAL STORAGE 7

1.4.1 Light metal hydride 8

1.4.2 Complex "hydridic" hydrides, borohydrides and alanates ($[BH_4]^-$ and $[AlH_4]^-$) 10

1.4.3 Complex "protonic hydrides"; nitrides, imides and amides 14

1.4.4 Ammonia-borane and amido-boranes 16

1.5 PHYSICAL STORAGE 19

1.6 STRATEGIES FOR THE IMPROVEMENT IN COMPLEX HYDRIDES 20

1.6.1. Hydride Destabilization 20

1.6.2. Catalytic effect in complex hydrides 22

1.6.3. Tuning small ion mobility in complex hydrides 23

1.7 LITHIUM-NITROGEN-HYDROGEN SYSTEM FOR HYDROGEN STORAGE 24

1.8 OBJECTIVE OF THIS THESIS 25

CHAPTER 2 27

EXPERIMENTAL METHODOLOGY 27

2.1 SAMPLE PREPARATION 28

2.1.1 Starting materials 28

2.1.2 Sample preparing for investigating the reaction mechanism in Li-N-H system 28

2.1.3 Sample preparing for synthesizing catalyst 29

2.1.4 Sample preparing for analyzing catalytic effect 30

2.2 SAMPLE CHARACTERIZATION 30

2.2.1 X-ray diffraction (XRD) 30

2.2.2 Transmission electron microscopy observations 32

2.2.3 Plastic bag method in TEM observations 33

2.2.4 X-ray photoelectron spectroscopy 36

2.2.5 Alternating current impedance 37

2.2.6 Thermo-gravimetry, differential thermal analysis and thermal gas desorption mass spectrometry 38

CHAPTER 3 41

REACTION MECHANISM OF DE/HYDROGENATION IN LI-N-H SYSTEM 41

3.1 BACKGROUND AND PURPOSE 41

3.2 EXPERIMENTAL PROCEDURES 42

3.3 RESULTS AND DISCUSSIONS 42

3.3.1 The formation site of LiH and LiNH2 during the de/hydrogenation process 42

3.3.2 The position and state of Ti compounds 46

3.3.3 Catalytic effect and decomposition mechanism model 49

3.4 CONCLUSIONS 50

CHAPTER 4 53

MECHANISM OF CATALYTIC EFFECT IN LI-N-H SYSTEM 53

4.1 BACKGROUND AND PURPOSE 53

4.2 EXPERIMENTAL PROCEDURES 54

4.3 RESULTS AND DISCUSSION 55

4.3.1 Synthesizing catalyst for the Li-N-H system 55

4.3.2 Thermal desorption properties of sample with catalyst 56

4.3.3 The appropriate amount of catalyst 58

4.3.4 The stability of catalyst state 60

4.4 **CONCLUSIONS** 64

CHAPTER 5 67

EFFECT OF LITHIUM ION CONDUCTION ON HYDROGEN DESORPTION IN LI-N-H SYSTEM 67

5.1 BACKGROUND AND PURPOSE 67

5.2 EXPERIMENTAL PROCEDURES 69

5.3 RESULTS AND DISCUSSION 69

5.4 CONCLUSIONS 74

CHAPTER 6 75

CONCLUSIONS AND PROSPECTS 75

6.1 OVERVIEW 75

6.2 SOLID-STATE REACTION MECHANISM IN LI-N-H SYSTEM 76

6.3 CATALYTIC MECHANISM IN LI-N-H SYSTEM 77

6.4 RELATIONSHIP BETWEEN THE CATALYTIC EFFECTS AND LITHIUM IONIC MOBILITY 77

6.5 PROSPECTS OF FUTURE WORK 78

REFERENCES 81

ACKNOWLEDGEMENTS 91

Chapter 1

Introduction

Why hydrogen?

The evaluation of the world energy consumption will be double over the next half century.[1] At the starting point of the 21st century it should be realized that there is an emergency requirement for an independent and sustainable energy carrier to substitute fossil fuels.[2, 3, 4] Meeting this demand will be challenging, and this would have a great influence on both energy structure and global warming. One of crucial steps in this process will be changing our dependence on carbon-based fossil fuels.[5]

Hydrogen is a kind of independent carrier in comparison to conventional ones, including fossil fuels. It accompanies following advantages such as clean, environmental friendliness and forming water as a non- polluting product during practical applications. Accordingly, reductions of dependence on fossil fuels and emissions of pollutants and greenhouse gases could be realized after using hydrogen as a primary fuel successfully.

Hydrogen is the most abundant element on Earth, but less than 1 % is represent as molecular hydrogen gas H_2. The overwhelming majority formed as H_2O in water. Some hydrogen always combines with carbon as liquid or gaseous hydrocarbons. Hydrogen is the ideal energy carrier for both mobile and stationary applications while averting adverse effects on the environment, and reducing dependence on imported fossil fuels for countries without natural resources. Electric energy, either from renewable energies, for example, wind, solar, and future fusion reactors, can be used to produce hydrogen from water by electrolysis. The consumption of hydrogen only formed water and the cycle is closed. Table 1.1 gives the energy density of common energy storage materials.[6] The energy density of hydrogen is the highest, twice higher than gasoline, which is the main fuel for daily life. Hence, hydrogen is the most attractive energy carrier. It needs to be developed today to facilitate the transition to a sustainable, carbon-neutral economy tomorrow.

Table 1.1: Energy densities of common energy storage materials

Storage material	MJ per kilogram	Direct use
Hydrogen (compressed at 70 MPa)	123	Fuel cell engines
Gasoline (petrol)	46	Automotive engines
Propane	46.4	Daily life/ automotive engines
Coal	24	Power plants
Wood	16.2	Heating
Lithium-ion battery	0.72	Computers/mobile phone

1.1 Hydrogen storage background

The greater hydrogen energy picture centres on the storage of hydrogen, the most significant step that currently present a bottle neck to utilization of hydrogen more widely in fuel cell systems. It should be realized that hydrogen is not naturally available. Recently hydrogen energy has been actively investigated in terms of production, storage and application (comprising combustion engines in vehicles and power application).[7] However, a safe, economic and efficient storage medium is like to be a crucial prerequisite before hydrogen would be globally used as a fuel, especially in practical

applications. Nowadays, compressed gaseous hydrogen is used in prototype and liquid form in advanced tan systems.[8] However, storing hydrogen in solid-state materials has definite advantages on accessible hydrogen content and energy efficiency compared to complex system that use high-pressure gas or cryogenic liquid. Solid-state storage of hydrogen is potentially superior with regard to its storage capacity (both gravimetric and volumetric), energy efficiency and safety.[3] Last but not least, storage of hydrogen in a solid medium is the most challenging and important part of realizing the hydrogen economy in the future applications (Figure 1). Therefore, hydrogen storage is a key point where actively international effort is made.

Figure 1. Alternatives for storing 4kg hydrogen in different state, with relatively volume in the size of a car (Image from Toyota press information, 33rd Tokyo Motor Show, 1999).

The US Department of Energy (US-DOE) set a criterion for vehicular applications in the following factors: hydrogen storage capacity; the amount of hydrogen stored per unit mass and per unit volume; fast kinetics; reversibility; etc.[9] During the past decade

(1998-2009), many researchers have investigated the hydrogen storage materials day and night in order to meet the requirements for practical applications. A series of storage materials have been proposed, such as metal hydrides and complex hydrides. Extensive efforts are currently being made for the improvement of hydrogen storage properties by improving the absorption/desorption kinetics, reducing the high thermal stability, and improving the purity of the desorbed hydrogen gas.[10]

1.2 Compressed hydrogen

The gaseous state of hydrogen kept under pressure is compressed hydrogen. This is the most popularly and technically used for mobile hydrogen storage in fuel cell vehicles. Normally, the pressure of compressed hydrogen in tanks is at 350 bar or 700 bar (Figure 2). Suzuki hydrogen fuel cell powered vehicles have introduced this kind of tank in Japanese market.

The only emission of hydrogen car is water vapor, which is environmental friendliness to the natural. This could help change the energy structure and boost hydrogen economy. However, like two sides of the coin, hydrogen tank does have disadvantage together with the advantages. The hydrogen requires to be stored in a highly compressed gas form, however if it breaks in to the environment then it would give rise to many danger situations. Moreover, the density of the volumetric is still not high. The energy densities are about 0.023 kg H_2 per liter tank volume.[11] Researchers

are currently developing safe, light-weight, composite materials for new compressed gas storage system.

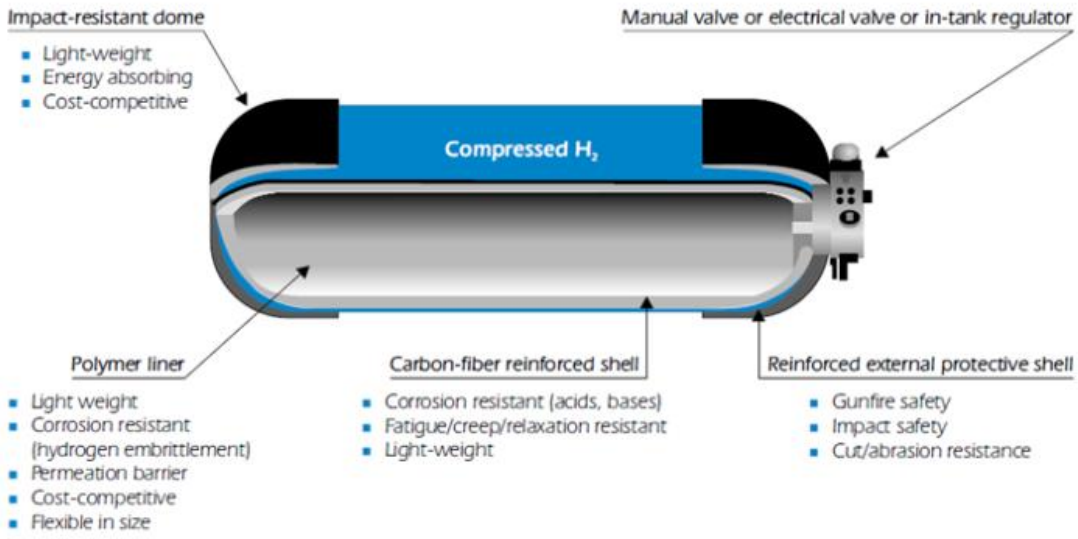

Figure 2. Schematic of hydrogen tank system from Quantum Technologies.

1.3 Liquefied hydrogen

The density of liquefied hydrogen is higher than gaseous hydrogen and it could contain more energy in a fixed volume. The same size tank can store more liquid hydrogen rather than gas hydrogen. Furthermore, the energy density is 8.4 MJ per liter twice the density of compressed hydrogen. However, the tank insulations demand to prevent hydrogen loss adds to volume, weight, and cost. Many automobile companies are working with on board liquid hydrogen for vehicles (Figure 3).

Figure 3. BMW's H2R (Hydrogen Record Car) is powered entirely by the clean-burning process of liquid-hydrogen combustion.

1.4 Chemical storage

The chemical storage of atoms hydrogen concerns materials where hydrogen is bound tightly with other elements in a compound. Hence, the loading and uploading of hydrogen (hydrogenation-dehydrogenation) may make it possible to store larger quantities of hydrogen in smaller volumes than gas or liquid hydrogen. In contrast,

physisorption is responsible in cases where molecules hydrogen is only physically absorbed on the surface of a solid or in the internal volume of porous/framework structures.

Among chemical storage materials, families of metal alloys and their hydrides constitute a core grouping that has been widely investigated for over a century.[12, 13, and 14] In general, the storage capacities of these materials are too low to satisfy the DOE targets for practical applications. However, it could find utility instationary applications due to the reversibility. For example, Mg_2Ni and $LaNi_5$ are two classic alloys that are remarkable due to their particular cycleability.[14] Nowadays, scientists are investigating several different kinds of materials, including light-metal hydrides and complex hydrides. Among them, the magnesium hydrides[15], borohydrides[5, 16, 17, and 18], alanates[19], and amides[20-24] are close to meeting US-DOE targets in terms of storage capacity, reversibility, cost and toxicity. The complex hydrides separate into two groups depend upon their composition and bonding: borohydrides and alanates, such as $LiBH_4$ and $LiAlH_4$, are hydridic in natural and contain hydrogen within complex anions that can be represented as H^-. By comparison, the imides and amides, for example Li_2NH, $LiNH_2$ are protonic and contain hydrogen within complex anions that can be expressed as H^+. These characters of complex hydride are covered separately in the sections below.

1.4.1 Light metal hydride

In a metal hydride the other element (usually one of the alkali metals or alkaline earth

metals) is a metal more electropositive than hydrogen. The hydrides are called binary if they only involve two elements including hydrogen. Chemical formula for binary ionic hydrides (where the generic metal's chemical symbol is represented as "M") are either MH (as in LiH) or MH_2 (as in MgH_2).[25] Among these light metal binary hydrides, magnesium hydride (MgH_2) is the most attractive because of its low atomic weight, high hydrogen storage capacity and low cost.[26, 27] In table 1.2, the gravimetric and volumetric density along with hydrogen desorption temperature and reversibility for selected light binary hydrides are compared with that of gaseous and liquid hydrogen.[12, 26-28] Even though MgH_2 has a high gravimetric capacity of 7.6 wt. %, it has limitations on the slow kinetics and a high decomposition temperature (up to 330 °C). A lot of researchers have been devoted to enhancing its performance.[29-40]

Table 1.2 Hydrogen content of simple binary hydrides in comparison with gaseous and liquid hydrogen. T_{dec} and kinetic reversibility of the hydrides are also given.

Compound	Wt. % H_2	Volumetric density N_H (atoms H/ml x 10^{-22})	T_{dec} (°C)	Kinetic reversibility
H_2, liquid	100	4.2	——	——
H_2, gas (100 atm)	100	0.49	——	——
LiH	12.6	5.3	720	Poor
NaH	4.2	2.3	425	Good
CaH_2	4.8	5.1	600	Good
MgH_2	7.6	6.7	330	Very poor
AlH_3	10.0	8.84	150	Irreversible
TiH_2	4.0	9.1	380	——[a]

[a] No literature data available

1.4.2 Complex "hydridic" hydrides, borohydrides and alanates ($[BH_4]^-$ and $[AlH_4]^-$)

Hydrides including complex anionic units with light element, such as B and Al, bonding with a more electropositive cation like Li, Na, K and Mg, have been defined as so-called

"chemical hydrides". In these complex hydrides, the hydrogen within the anionic unit are covalently bonded to a central atom in an anion complex (e.g. $[AlH_6]^{3-}$, $[AlH_4]^-$ and $[BH_4]^-$) and stabilized by a cation, especially an alkali (e.g. Li) or alkaline earth metal (e.g. Mg), to form $LiAlH_4$, $LiBH_4$ and $Mg(BH_4)_2$. These materials are investigated due to their very large gravimetric and volumetric hydrogen densities (Table 1.3). However, their thermal stability and high desorption temperature often limit them for practical application.

Table 1.3 Desorption temperature and gravimetric storage capacities of complex chemical hydrides[3, 16]

Compound	T_{des} (°C)	Storage capacity (wt. %)
$LiAlH_4$	125	9.5
$LiBH_4$	380	18.4
$NaAlH_4$	210	7.4
$NaBH_4$	400	10.6
$KAlH_4$	270	5.7
KBH_4	500	7.4
$Mg(AlH_4)_2$	140-200	9.3
$Mg(BH_4)_2$	260-280	14.8
$Ca(AlH_4)_2$	250[a]	7.8
$Ca(BH_4)_2$	320	11.5
$Al(BH_4)_3$	20	16.8

[a] For complete desorption from neat $Ca(AlH_4)_2$.[41]

Alanates have received a lot of attention over the past decade, which can be classified as hexahydroaluminates or tetrahydroaluminates. A comprehensive summary of the well-known structures of all aluminum-based hydrides was recently prepared by Hauback.[42] Among these materials, sodium alanate with catalyst ($NaAlH_4$ + 2 mol % Ti)[43] is the most well studied reversible complex hydrides in the following reaction:

$$3NaAlH_4 \leftrightarrow Na_3AlH_6 + 2Al + 3H_2 \leftrightarrow 3NaH + Al + 9/2H_2 \quad (1)$$

After doping a few mol % Ti in the complex metal hydride, the discovery of reversibility in the complex hydride was a breakthrough in solid-state hydrogen storage. The catalyzed sodium alanate system exhibits lower dehydrogenation temperature, better kinetics and larger reversible hydrogen capacity. Recently, some researchers have demonstrated reversible hydrogen cycling in Ti-catalyzed sodium alanate over 100 cycles with a measured capacity of nearly 4 wt. % at 160 °C.[44] Although the capacity and cycling properties of catalyzed sodium alanate are unlikely to ever meet all of the DOE targets, there is still much interest in trying to understand the mechanism behind the low-temperature reversibility in this system. This is an indication that Ti worked effectively for solid-state $NaAlH_4$. Interest in using complex metal hydride as hydrogen storage materials has dramatically reawakened.

The groups of complex hydrides that have been investigated actively during the last

ten years are the borohydrides, which could absorb a large amount of hydrogen. The crystal structures of the various borohydrides have been studied by Orimo et al.[16] Normally, the alkali borohydrides require prohibitively high temperature for H_2 desorption and have a large decomposition enthalpy. As a representative borohydride, $LiBH_4$, with a hydrogen capacity of 13.5 wt. %, has been well studied in the following reaction:

$$2LiBH_4 \rightarrow 2LiH + 2B + 3H_2 \quad (2)$$

During this reaction, LiBH4 desorbs hydrogen at temperatures more than 380 °C due to the high thermodynamic stability. In order to reduce the decomposition enthalpy, some effort is focusing on introducing a second species to destabilize the structure of $LiBH_4$.[45-47] What is more, other effort improves the reaction kinetics from the standpoint of the size of $LiBH_4$ powders.[48]

In addition, Fang et al. reported a chemical activation of $LiBH_4$ by ball-milling with TiF_3 that can rapidly release 5.7 wt % hydrogen at moderate temperature without any other by-product gas.[49] However, the isothermal desorption profiles showed that it takes an hour to fully release the H_2. There remain ample opportunities for further performance optimization and certainly there is a need to understand much more regarding the catalytic processes involved in Ti doping to alanates and borohydrides.

1.4.3 Complex "protonic hydrides"; nitrides, imides and amides

Another series of materials that have received much attention in recent years is the amide-imide system. The crystal structures of the various amides and imides of interest can be found in the review by Orimo et al. [16]and references therein. The reversible reaction could desorb hydrogen through reaction between amide and hydride. Since it was first reported by Chen et al.[50] in 2002 (Figure 4), the lithium-nitrogen-hydrogen system has been investigated, due to its light weight and relatively high H_2 storage capacity. Lithium amide absorbs and desorbs a large amount of hydrogen in the two consecutive reactions as follows:

$$LiNH_2 + LiH \leftrightarrow Li_2NH + H_2 \quad (3)$$

$$Li_2NH + LiH \leftrightarrow Li_3N + H_2 \quad (4)$$

Theoretically, a large amount (11.5 wt. %) of hydrogen is accessible in these two reactions. Ichikawa et al. chose $LiNH_2$ and LiH as starting materials and investigated the hydrogenation and dehydrogenation characteristics of the mixture.[51-55] This is because reaction (3), which can provide a theoretical hydrogen storage capacity of 6.5 wt. %, has a relatively low enthalpy of reaction and a reasonable hydrogen pressure of 1 bar at 285 °C.[56] However, this reaction requires high temperatures for complete desorption and is therefore not practical for many applications. Therefore, current efforts have been devoted to decrease the desorption temperature, and to clarify the

decomposition mechanism of $LiNH_2$ and LiH.

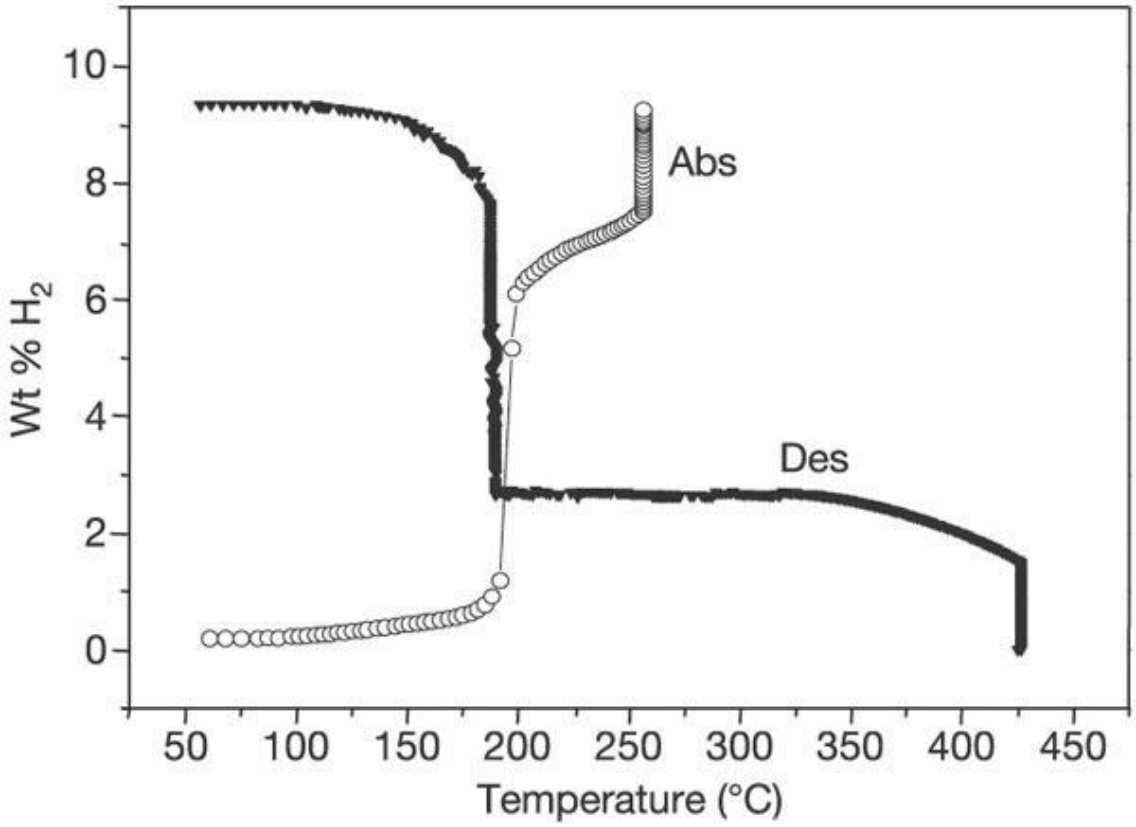

Figure 4. The absorption process (Abs) and desorption process (Des) for lithium nitride-imide-amide system (Reprinted from ref. 50).

An alternative approach uses lithium hydride and magnesium amide in a similar reaction:[57]

$$Mg(NH_2)_2 + 2LiH \leftrightarrow Li_2Mg(NH)_2 + 2H_2 \quad (5)$$

Reaction (5) has a theoretical hydrogen content of 5.6 wt. % and has been shown to release H2 at much lower temperature than the lithium amide reaction.[57] However, the dehydrogenation temperature remains too high for low-temperature fuel-cell

applications. Moreover, the nitrogen-based hydrides have a tendency to produce ammonia along with hydrogen during high temperature desorption. The main reason is because $LiNH_2$ decomposes at higher temperatures. The loss of nitrogen exhausts the starting materials and leads to reduce capacity of hydrogen. More importantly, ammonia is a poison for hydrogen system and must be completely got rid of the hydrogen fuel. Currently researchers pay more attention to add catalyst to promote decomposition reaction pathways that avoid ammonia formation.[16]

1.4.4 Ammonia-borane and amido-boranes

Nowadays, Ammonia-borane (NH_3BH_3, AB) is considered to be an attractive candidate within theoretically 19.6 wt. % of H_2 due to its safety features.[58-64] Shore et al. first synthesized NH_3BH_3 which is stable at ambient temperature in 1955.[65] In the context of amide-hydride destabilization combining the protonic and hydridic hydrogen, NH_3BH_3 is a remarkable compound in that both hydridic B-H and protonic N-H bonds exist within the same structure.[66] Being nonflammable and nonexplosive under standard condition, it undergoes a two-step decomposition under low temperature range from 70 to 200 °C, releasing ~6.5 wt. % of hydrogen at each step: Polyaminoborane, $[NH_2BH_2]_n$, is yielded with hydrogen release in the first step, which reaches a maximum at ~130 °C; The second step, forming polyiminoborane, $[NHBH]_n$, occurs in the range of 150-200 °C. At much higher temperature up to 500 °C, the

decomposition chain can be even carried all the way through to boron nitride with further hydrogen release. The decomposition process can be described as follows:

$$nNH_3BH_3 \rightarrow [NH_2BH_2]_n + nH_2 \quad (6)$$

$$[NH_2BH_2]_n \rightarrow [NHBH]_n + H_2 \quad (7)$$

$$[NHBH]_n \rightarrow nBN + nH_2 \quad (8)$$

However, there still some problems need to be realized for AB in the practical applications. First of all, the decomposition temperature is still higher than the DOE target (85 °C). Moreover, some undesirable by-products like ammonia, borazine and diborane are detected during dehydrogenation. These undesirable gases could either poison the hydrogen production or cause safety problems during application. Last but not least, the final solid-product, BN, is chemically too stable to be recycled at ambient temperature.

Recently, a significant development in the hydrogen release temperature has been reported by Xiong et al.[67] in alkali-metal amidoboranes, $LiNH_2BH_3$ and $NaNH_2BH_3$, releasing 10.9 wt. % and 7.5 wt. % of hydrogen, respectively, at ~90 °C via:

$$nLiNH_2BH_3 \rightarrow (LiNBH)_n + 2nH_2 \quad (9)$$

$$NNaNH_2BH_3 \rightarrow (NaNBH)_n + 2nH_2 \quad (10)$$

In addition, the composites do not release unwanted borazine by-product and the

reactions are devoid of lengthy induction periods and foaming (Figure 5). Despite the several advantages of ammonia-borane and amidoborane systems, the most serious drawback is the lack of facile reversibility which makes them inappropriate for on-board applications. These materials could possible serve as an alternative to other complex hydrides as a sustainable hydrogen storage medium with an efficient regeneration process.

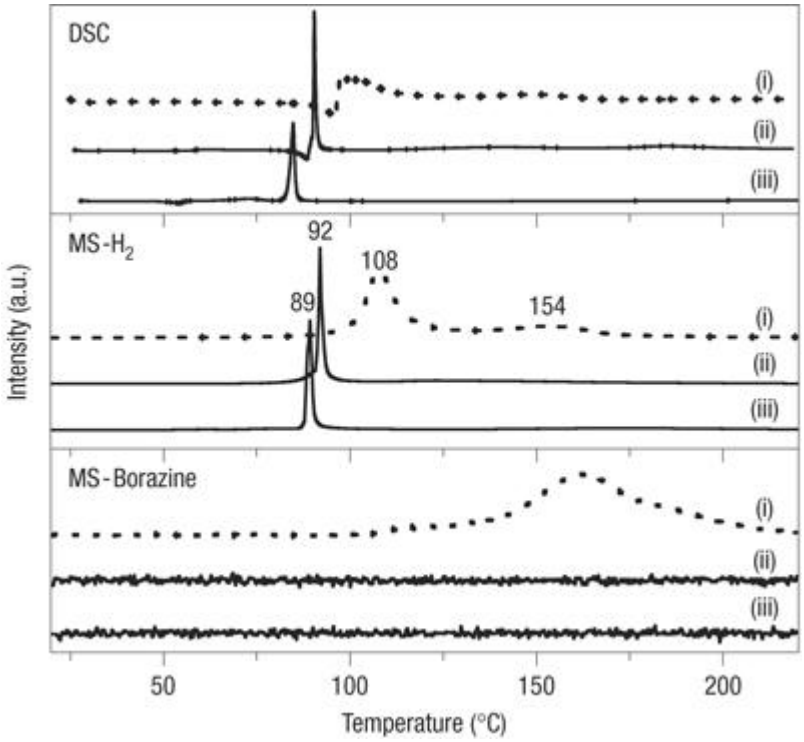

Figure 5. Mass spectra of gas desorption: (i) post-milled ammonia borane; (ii) Li amidoborane sample; (iii) Na amidoborane sample (Reprinted from ref. 67).

1.5 Physical Storage

Unlike chemical storage where the hydrogen is held chemically to component atoms within a solid structure, in physical storage systems the hydrogen is attached in a surface or porous of a solid material without dissociation. Examples of materials, such as coordination polymers, metal organic frameworks (MOF's), polymers with intrinsic microporosity (PIMs), activated carbons (Figure 6) and zeolites, have been widely investigated for hydrogen storage via physisorption.[68] Weak van der Waals interactions are responsible for the absorption of H_2 between gas molecules and the surface of host materials. Therefore, hydrogen absorption happens at very low temperature. Later reported reproduction showed that only 0.6 wt. % hydrogen could be absorbed by single-wall carbon nanotubes at room temperature.[69, 70] However, activated carbon with a high specific surface area could absorb 4.5 wt. % of hydrogen at 77K.[71] Considering of this situation, the application for activated carbon materials is still limitation by hydrogen capacity.

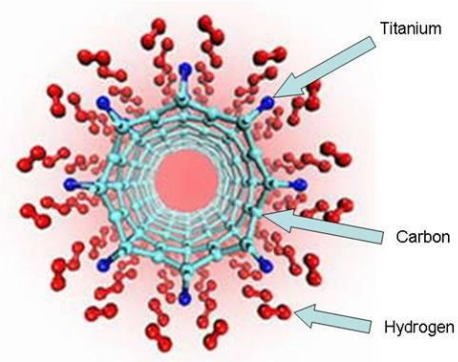

Figure 6. Physisorption of hydrogen through carbon nanotube catalyzed by titanium.

1.6 Strategies for the improvement in complex hydrides

Complex hydrides are investigated actively due to their properties of safe, efficient and reversible for on-board hydrogen storage. These materials have higher gravimetric and volumetric hydrogen densities than the pressurized gaseous or cryogenically liquefied hydrogen. However, complex hydrides have one or more limitations for practical applications: 1) slow reaction kinetics, 2) relatively high thermal stability, 3) irreversibility on cycling, 4) undesirable by-product gases.[7, 12] Therefore, different approaches for the improvement of hydrogen storage properties in complex hydrides have been studied from improving the absorption/desorption kinetics, decreasing the decomposition temperature, purifying the desorbed hydrogen gas.[10]

1.6.1. Hydride Destabilization

The stability of some light-weight hydrides is too high for desorption/absorption hydrogen at practical temperatures and pressures due to their strongly bound between the cation and anion.[16,19] For example, LiH has a high hydrogen capacity of 12.5 wt. %. However, it needs a desorption temperature of 910 °C at an equilibrium pressure of 1 bar.[72] An approach to decrease the dehydrogenation temperature of these stable hydrides is to destabilize them through alloy formation upon dehydrogenation by doping additives.[73, 74] The dehydrogenation product could form alloy instead of the element metal, because the cohesive energy of the alloy forms between the additives and the

metal. In this case, the dehydrogenation enthalpy is reduced dramatically. Herein, we discuss the positive effect of lithium hydride with silicon.

Silicon is a relatively light-weight semi-metal, which can destabilize alkali and alkaline-earth metal hydrides like LiH, MgH_2[73, 74] and CaH_2[75-77]. It can combine with these light metals and form stable alloy easily. Herein, we use LiH as an example. After doping silicon in LiH, various Li_xSi_y alloys formed and the dehydrogenation enthalpies are decreased to approximately 120 $kJmol^{-1}$. Furthermore, the desorption temperatures at 1 bar equilibrium pressure are lower to 470 °C (Figure 7).

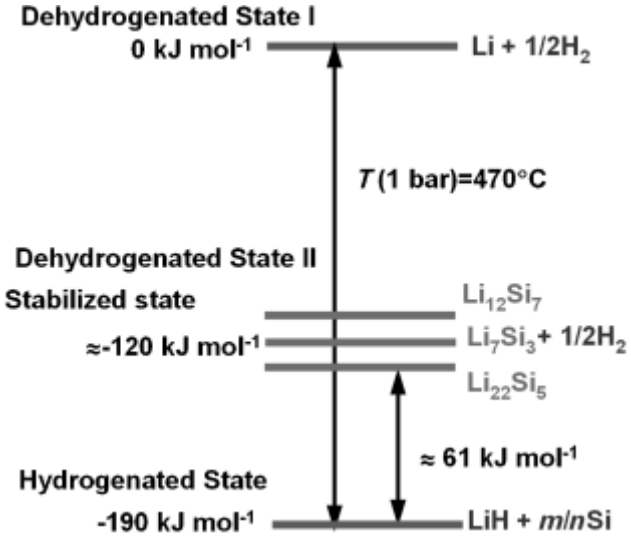

Figure 7. The formation of lithium-silicon alloys help reduce the dehydrogenation enthalpy significantly (reprinted from ref.10).

However, the additional silicon could cause the hydrogen capacity reducing to 2.8-7 wt. %. Moreover, some researchers found a new ternary phase Li_4Si_2H is formed with relatively high stability after rehydrogenation. The new ternary hydride leads to an

incomplete dehydrogenation which also reduces the hydrogen capacity.

1.6.2. Catalytic effect in complex hydrides

Extensive efforts are currently being made to approach for the improvement of hydrogen storage properties on improving the absorption/desorption kinetics, reducing the operating temperatures and improving the purity of the desorbed hydrogen gas. One of strategies for the improvement of the hydrogen storage properties is addition of catalyst. Ti compounds have been well known to catalyze the dehydrogenation of complex aluminium hydrides in solution. Wieberg et al. firstly in 1951 observed Ti catalysed dehydrogenation of $LiAlH_4$ in a diethyl ether suspension.[78] A breakthrough came when Bogdanović and Schwickardi certificated that doping a few mol % Ti in the complex metal hydride $NaAlH_4$ lowered the dehydrogenation temperature, improved the kinetics and allowed rehydrogenation of the decomposition products.[79] This is indication that Ti worked effectively for the solid-state $NaAlH_4$. Interest in using complex metal hydrides as hydrogen storage materials is dramatically reawakened. MgH_2 exhibits a high hydrogen capacity up to 7.6 wt %. However, the absorption and desoption reaction of Mg/MgH_2 itself is too slow. Barkhordarian et al. reported that Ti compounds had a catalytic effect for absorption and desorption.[36, 80, 81] Subsequently, Hanada et al. reported the valence state of the Ti compounds which doped in MgH_2.[82] Meanwhile, the catalytic effect of Ti compound was also found in $LiH/LiNH_2$ system which could be reversibility and have a high hydrogen capacity of 6.5 wt %.[83] The

absorption/desorption kinetics and the purity of the desorbed hydrogen gas had been improved. However, the catalyst state of Ti compound is not as same as the original after ball-milling and/or heat treatment. [83, 84] In this case, the mechanism of catalytic effect is difficult to understand clearly due to the instability of Ti compounds.

1.6.3. Tuning small ion mobility in complex hydrides

The de/hydrogenation for complex hydrides is kind of solid-state reaction, which include solid-solid reaction, solid-liquid reaction and solid-gas reaction. Diffusion plays an important role in solid-state reactions, as they require the coming together of reactive species. Their rigid structures make solids different from liquids and gases. The kinetics of solid-state reactions is therefore greatly dependent on the crystal structure and its defects.

Recently, oxide-electrolyte-materials with a special structure, such as spinels, perovskites, and fluorites, have been investigated actively due to the characteristics of mobile interstitial ions and/or vacancies. The mobile species can be either cations or anions. Considering of the solid-state reaction of complex hydrides, the mobile species of cations or anions also play a significant role in the improvement of kinetics. Therefore, it is of reasonable interest to draw essence from the well-established oxide-electrolyte-systems, and provide the structural characteristics of these faster ionic materials to the complex hydrides systems in order to accelerate the reaction kinetics.

One possible structural type that might accelerate hydrogen mobility is perovskite. In

this structure, the oxygen ionic conductivity exhibit very high and can be used as proton conductors.[85-87] Accordingly, some researchers have studied the hydrogen storage properties of $NaMgH_3$ which has the perovskite structure.[88, 89] The hydrogen mobility in $NaMgH_3$ is higher than that in MgH_2, which help improve the reaction kinetics during de/hydrogenation process.[90-92] Among these approaches for improved properties, the tuning of small ion mobility has some priorities. It does not reduce the hydrogen capacity, improves the reaction kinetics and decreases the dehydrogenation temperature.

1.7 Lithium-Nitrogen-Hydrogen system for hydrogen storage

Since the first time reported by Chen et al. in 2002, Li-N-H system have been investigated with their reversibility and relatively high H_2 storage capacity.[50] As the result of their investigation, hydrogen can be desorbed via the following reaction:

$$LiNH_2 + LiH \leftrightarrow Li_2NH + H_2, \quad (1)$$

Theoretically, a large amount (6.5 wt. %) of hydrogen is accessible in this reaction. However, the system is still limited by high desorption temperature and slow reaction kinetics for practical applications. It is well-known that NH_3 is a subsidiary product for the dehydrogenation of the Li-N-H system according to the following reaction:

$$LiNH_2 \rightarrow Li_2NH + NH_3, \quad (2)$$

The main reason is because $LiNH_2$ could decompose at higher temperature.

To date, catalyst has been found from the standpoint of kinetics, such as $TiCl_3$, Si, and BN.[51,53,93,94] After these endeavors, H_2 desorption temperature has been decreased. However, $TiCl_3$, being doped as the catalyst, accompanied following characteristics such as flammability, spontaneous combustion and poison. Because the whole system will absorb/desorb H_2, safety and environmental friendliness must be considered as one of the most important factors. At the same time, $TiCl_3$ is not stable in Li-N-H system during high-energy ball milling and heat treatment. Si and BN is stable under experimental atmosphere, whereas the desorption temperature of the sample with Si or BN is not as low as that with $TiCl_3$. Hence, new appropriate catalyst should be searched out. David et al. proposed in their report that the reaction based on Li^+ migration across reactive interfaces in equation (1).[95] Based on these results, it could be deduced that the kinetics of this reaction might be improved due to the increasing activity of Li^+ ions.

1.8 Objective of this thesis

As shown in the previous section, lithium-nitrogen-hydrogen system has been well studied as hydrogen storage materials, since its relatively high capacity of hydrogen and good reversibility during de/hydrogenation. Furthermore, the cost of starting materials is lower than fossil fuels. However, there still have some parts not clearly in this system. Firstly, the reaction mechanism in nano scale between lithium hydride and lithium amide is still need to be investigated in details. To date, little evidence could be acquired

from the recent literature showing the position and phase change between each solid phase. Moreover, previous research has shown that some catalysts, especially titanium compounds, have an effect on improving both the hydrogen absorption and desorption kinetics of this system. However, the catalysts which are effective for the de/hydrogenation in the nano scale have not yet been clearly understood. Last but not least, according to the previous approach, from the standpoint of the tuning of small ion mobility, one attempt to enhance the hydrogen-storage properties of the Li-N-H system is to target a catalyst that would effectively increase the mobility of the Li^+ ions.

In the following chapters, these targets will be studied on the basis of a series of experiments. The conclusion will be carefully shown after discussions.

Chapter 2

Experimental Methodology

This chapter covers the experimental techniques and equipment used during this study, a description of the material and its condition as well as the experimental procedures including details about the sample preparations for each technique. A variety of characterization equipment were used, including a pressure-composition-isotherm (PCI) device, a X-ray diffraction (XRD), two kinds of transmission electron microscope (TEM),a X-ray photoelectron spectroscopy (XPS), a alternating current (AC)

impedance, a Thermo-gravimetry (TG), a differential thermal analysis (DTA) equipment and thermal gas desorption mass spectrometry (TDMS).

2.1 Sample preparation

2.1.1 Starting materials

The powder of $LiAlH_4$ (95 %), Li_2CO_3 (99.997%), $TiCl_3$, TiO_2 (99%), Ti_2O_3 (99.9%), LiH (95%) and $LiNH_2$ (95%) were purchased from Sigma-Aldrich. MgH_2 (98%) powder was purchased from Alfa Aesar.

2.1.2 Sample preparing for investigating the reaction mechanism in Li-N-H system

For the contrast experiment sample without catalyst, Li_2NH was prepared by using $LiNH_2$ in a pressure-composition-isotherm (PCI) device with a heating rate of 5 °C/min. This heat treatment was kept at 400 °C, 8 h under vacuum condition. After that, hand milling was conducted by using agate mortar to make the powder tiny.

On the other hand, for the sample with catalyst, Li_2NH was prepared in the same way as the sample without catalyst. And then 1 mol. % $TiCl_3$ was doped into the Li_2NH. In the high energy ball milling process, the powders and 20 pieces of steel balls with a diameter of 7 mm were brought into a Cr steel pot, and milled at 400 rpm for 2 h under

a hydrogen gas pressure of 1 MPa at room temperature. The ball-to-powder ratio was 100:1.

At last, the hydrogenation process was prepared by using the Li_2NH and Li_2NH with $TiCl_3$ in PCI device at 200 °C, under a H_2 atmosphere 1 MPa, respectively. The hydrogenation time was 1000 min. All the processes of sample preparation in this work were performed in an Ar glovebox (MDB-2BL, Miwa Mfg. Co. Ltd.) to avoid the sample pollution due to water and oxygen in air.

2.1.3 Sample preparing for synthesizing catalyst

The single phase of $LiTi_2O_4$ was synthesized by a two-step solid-state reaction. $Li_2Ti_2O_5$ will form as an intermediate compound.[96] The reaction equations used here are:

$$Li_2CO_3 + 2TiO_2 \rightarrow Li_2Ti_2O_5 + CO_2 \quad (4)$$

$$Li_2Ti_2O_5 + Ti_2O_3 \rightarrow 2LiTi_2O_4 \quad (5)$$

The synthesis method of $LiTi_2O_4$ is according to Xu et al. introduced before.[97] Considering the volatility of Li, it was hard to get the exact composition of Li. Here the excess molar fraction 0.15 of Li_2CO_3 is added in step (1) for $LiTi_2O_4$. An additional factor is sensitivity of $LiTi_2O_4$ to air. This issue was mentioned by several groups,[98-100] regardless of the preparation method used. The aging reaction is the topotactic oxidation of $LiTi_2O_4$. $LiTi_2O_4$ reacts with oxygen or H_2O in air and is progressively transformed into $Li_{1-x}Ti_2O_4$ ($0 \leq x \leq 0.8$). The polycrystalline sample is stored in Ar atmosphere in

order to avoid the aging reaction with oxygen and moisture.

2.1.4 Sample preparing for analyzing catalytic effect

Typically, to ensure homogeneous mixing between the starting materials and the additive, ball-milling equipment (Fritsch P7) was used. $LiNH_2$ and LiH powders (300 mg, 1:1.2 molar ratio) and $LiTi_2O_4$ (0.5 mol%) were milled for 2 h. Furthermore, different molar ratios of $LiTi_2O_4$ (0.5 and 2 mol%) were doped into the $LiNH_2$/LiH powders, which were milled for 2 h. In the high-energy ball-milling process, the powder and 20 steel balls (SUJ-2) with a diameter of 7 mm were brought into a Cr steel pot (SKD-11) and milled at 400 rpm for 2 h under a hydrogen gas (99.9999% purity) pressure of 1 MPa at room temperature. The ball-to-powder ratio was 100:1. The milling was interrupted every 1 h for 30 min to prevent frictional heat during the milling process. Samples of $LiAlH_4$ and 0.5 mol % $LiTi_2O_4$ were milled for 2 h. The samples, mixtures of MgH_2 and 1 mol % $LiTi_2O_4$, were milled for 20 h.

2.2 Sample characterization

2.2.1 X-ray diffraction (XRD)

X-ray diffraction is a tool used for identifying the phases of the samples and estimating the crystallite size. The theory of XRD is according to the phenomenon that the crystalline atoms cause a beam of X-rays to diffract into many specific directions. The

diffraction on different crystal planes follows the Bragg's Law, as shown in Equation 2.1:

$$2d\sin\theta = n\lambda \quad (2.1)$$

Here d is the spacing between diffracting planes, θ is the incident angle, n is any integer, and λ is the wavelength of the beam. These specific directions appear as spots on the diffraction pattern called refections. Thus, X-ray diffraction results from an electromagnetic wave impinging on a regular array of scatterers.

The Scherrer equation, in X-ray diffraction, is a formula that relates the size of sub-micrometer particles, or crystallites, in a solid to the broadening of a peak in a diffraction pattern. It is named after Paul Scherrer.[101-103] The crystalline size can be derived from the broadening of the XRD peaks. The Scherrer equation can be written as:

$$T = \frac{K\lambda}{\beta\cos\theta} \quad (2.2)$$

Where T is the mean size of the ordered domains, which may be smaller or equal to the grain size, K is a dimensionless shape factor, with a value close to unity. The shape factor has a typical value of about 0.9, but varies with the actual shape of the crystallite, λ is the wavelength of the beam, β is the line broadening at half the maximum intensity, after subtracting the instrumental line broadening, in radians, θ is the Bragg angle.

In this study, XRD experiment is performed using a Philips X'Pert Pro powder

diffractometer with Cu Kα radiation. The wavelength of the incident X-ray is 1.54 Å. The sample was set on a glass plate, and covered by a kapton sheet of 8 μm thickness sealed by the vacuum grease, in order to prevent oxidention during the measurements.

2.2.2 Transmission electron microscopy observations

Transmission electron microscopy (TEM) is a powerful method to characterize materials in micro or nano scale. It is an analytical method which allows detailed examination of microstructure, crystal structures, chemical compositions and orientation of precipitates, through bright field image, high-resolution image, diffraction pattern and X-ray analysis.

With the purpose of knowing the position formed of each solid phase, we have used TEM (JEOL 2010 200 KV and FEI Tecnai G^2 F20 200KV) to observe samples. The TEM samples were prepared by spreading the dry powder on a molybdenum grid in the glovebox. The grid had a 5 min heat treatment in vacuum condition to take off the deposit builder. The subsequent sample transferring and operation were performed in a specially designed Ar-filled plastic bag[104]. A heating holder of TEM was used for in-situ dehydrogenation process to observe the location of each solid phase.

The purpose of using the TEM of JEOL 2010 is to obtain bright field image, dark field image, and selected-area electron diffraction (SAED). The in-situ and ex-situ experiment is used by JEOL 2010. According to these, it is obviously to discover the

position of the $LiNH_2$/Li_2NH and LiH.

By using the TEM of FEI F20, high-angle annular dark field scanning transmission electron microscopy (HAADF STEM) image is obtained. The character of HAADF STEM image is that the contrast between high atomicnumbers and low atomicnumbers is apparently, such as Ti compounds and $LiNH_2$/LiH. It is a good method to observe the position of catalyst visually. And in addition, contemporary electron microscopy is equipped with an energy dispersive X-ray analysis (EDAX) detector. It enables both quantitative and qualitative analysis of the specimen to be obtained. This could be helpful to validate the state of catalyst.

In order to minimize the knock-off and heat damage caused by the radiation from the electron beam in TEM, the intensity of the electron beam was limited during the microstructure observations.

2.2.3 Plastic bag method in TEM observations

Additionally, in the transfer of the $LiNH_2$ and LiH to the TEM from the glove box, a transfer method employing a plastic bag was introduced.

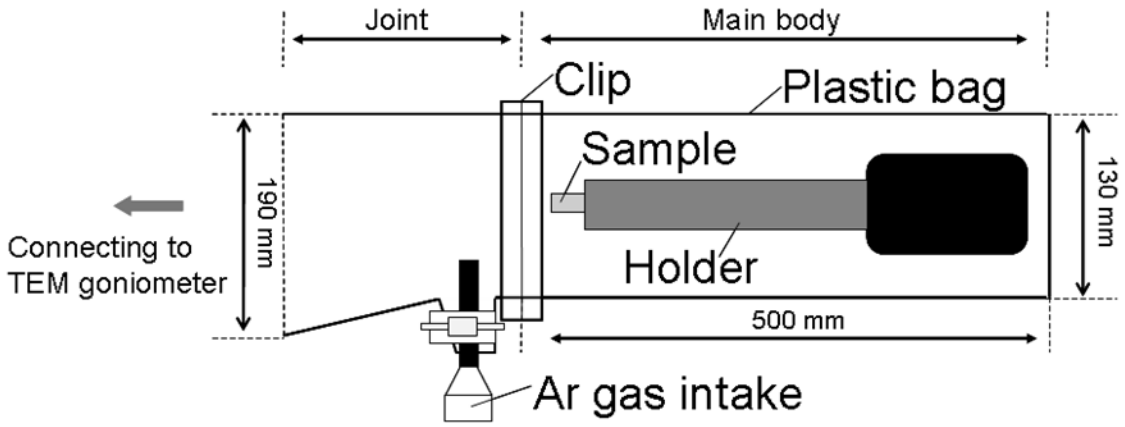

Figure 2.1. Schematic illustration shows what the plastic bag method is.

Figure 2.1 shows the illustration diagram of plastic bag method. The plastic bag is made of polyethylene and has a 0.040 mm in thick. It consists of main body and joints fabricated by heated wire welding. It should be guaranteed that the edge of bag is well-sealed with no leakage. In the glove box, the TEM holder can be sealed in the main body of plastic bag by a clip at the position between main body and joint section as shown in Figure 2.1. This can ensure that the TEM holder can be transferred to the TEM aside without any air exposure. And then the joint section of the plastic bag should be connected to the entrance of TEM by tape. With flushing argon gas (purity 99.999%) to the joint section at a pressure of 0.2 M Pa, the transfer from plastic bag main body to TEM can be done appropriately. Following 3-5 minutes of flushing gas, the holder can be loaded into the TEM with releasing the clip[1)]. It should be noted that the size of plastic bag method showed in Fig. 2.1 is not fixed and can be modified due to any type of TEM holders, such as a high voltage microscope.

Figure 2.2 shows the bright field image of Li_2NH after heat treatment, with the corresponding diffraction patterns and the dark field image. There is no clear indication of oxide or hydroxide particles in the bright-field image. The corresponding diffraction patterns obviously shows single crystal diffraction pattern which definitely demonstrate the monocrystalline structure in the matrix. Conversely, although slightly several diffraction rings from polycrystalline structure could be detected in diffraction patterns, it does not cause any misunderstanding or error to identification from diffraction patterns. Furthermore, Li_2NH has been identified from diffraction patterns and oxide or hydroxide diffraction spots/rings cannot be found. The dark field image shows obviously this particle is a single crystal of Li_2NH. These results indicate that plastic bag method was good enough to be used for sample observation without air exposure.

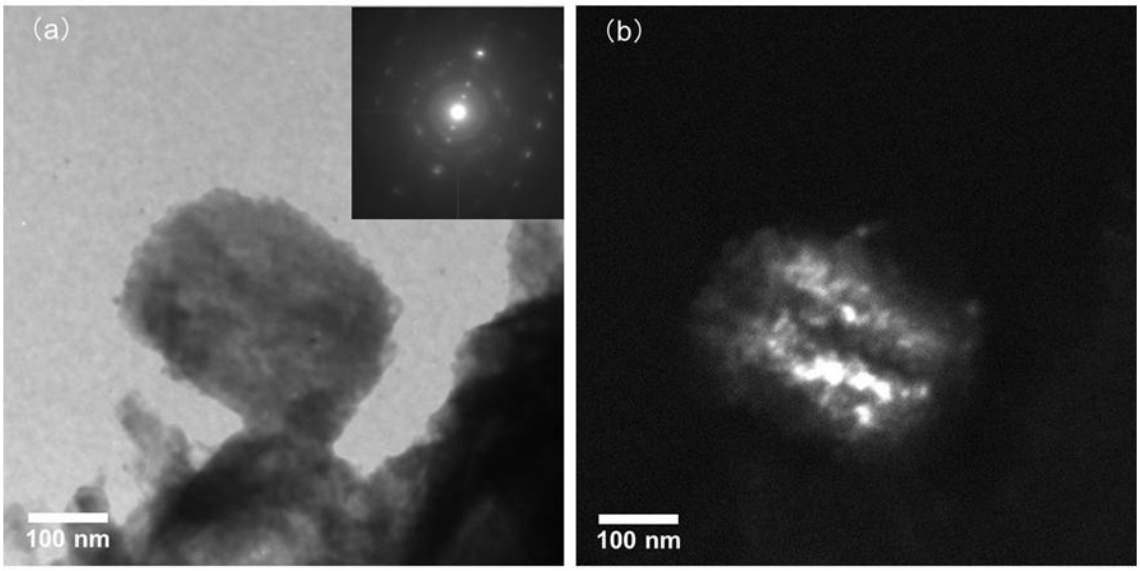

Figure 2.2. (a) Under the plastic bag method, low magnification of a bright-field image and corresponding diffraction patterns from Li2NH sample, (b) The dark field image.

2.2.4 X-ray photoelectron spectroscopy

X-ray photoelectron spectroscopy (XPS) is a surface-sensitive quantitative spectroscopic technique that measures the elemental composition at the parts per thousand range, empirical formula, chemical state and electronic state of the elements that exist within a material (Figure 2.3)[105]. XPS spectra are obtained by irradiating a material with a beam of X-rays while simultaneously measuring the kinetic energy and number of electrons that escape from the top 0 to 10 nm of the material being analyzed. XPS requires high vacuum (P ~10^{-8} millibar) or ultra-high vacuum (UHV; $P < 10^{-9}$ millibar) conditions, although a current area of development is ambient-pressure XPS, in which samples are analyzed at pressures of a few tens of millibar.

XPS is a surface chemical analysis technique that can be used to analyze the surface chemistry of a material in its as-received state, or after some treatment, for example: fracturing, cutting or scraping in air or UHV to expose the bulk chemistry, ion beam etching to clean off some or all of the surface contamination (with mild ion etching) or to intentionally expose deeper layers of the sample (with more extensive ion etching) in depth-profiling XPS, exposure to heat to study the changes due to heating, exposure to reactive gases or solutions, exposure to ion beam implant, exposure to ultraviolet light.

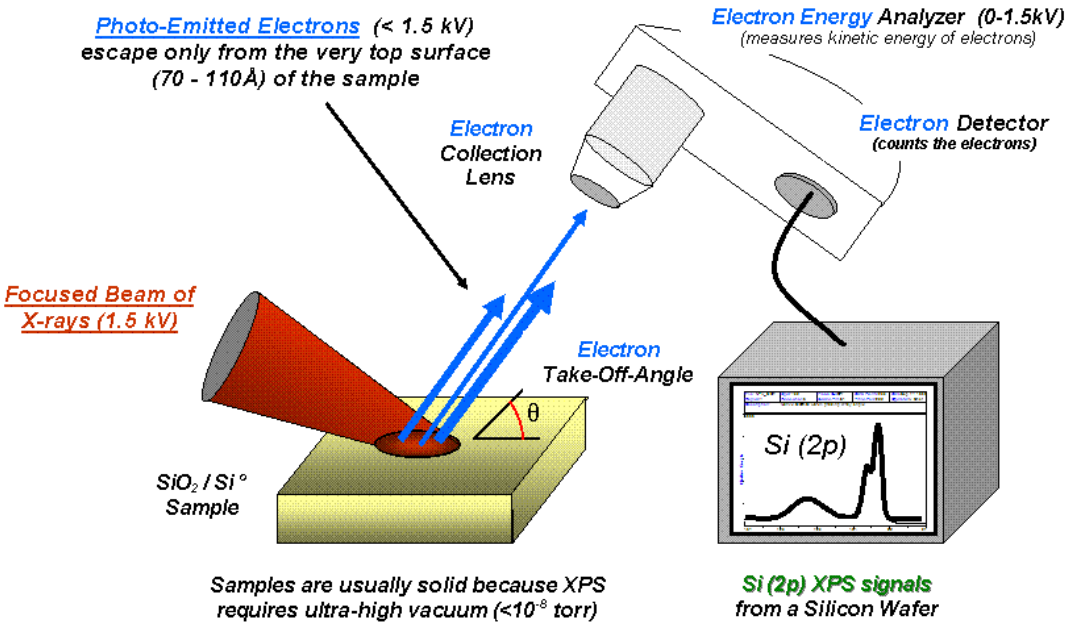

Figure 2.3. Basic components of a monochromatic XPS system.

In this study, X-ray photoelectron spectroscopy (XPS) measurement was carried out using a JPS-90MS photoelectron spectrometer with Mg Kα radiation.

2.2.5 Alternating current impedance

The electrical conductivity was measured by ac complex impedance method by a Solartron SI-1260 impedance analyzer in a frequency range from 1 Hz to 10 MHz under the control of a PC (Figure 2.4). The sample disks (8 mm in diameter and ca. 1.5 mm in thickness) formed by pressing the powdered material were sandwiched between

lithium-metal electrode and set in a 2-electrode cell in the glove box filled with purified argon. The cell was placed in a thermostatic oil bath in order to control the temperature. Temperature ranges for the measurement were from RT to above and below reaction temperatures for $LiNH_2$ and LiH mixture. The observed impedance data were analyzed as a conventional method for evaluating the electrical conductivity from the diameter of a single arc observed on the impedance plot.

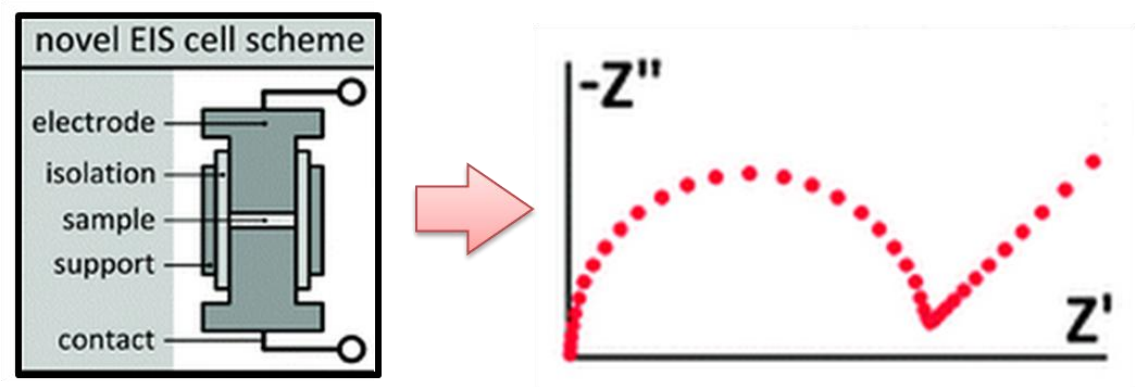

Figure 2.4. Electrical impedance cell scheme (left) and typical impedance plots (right).

2.2.6 Thermo-gravimetry, differential thermal analysis and thermal gas desorption mass spectrometry

Thermo-gravimetry and differential thermal analysis (TG-DTA) is a method of thermal analysis in which changes in physical and chemical properties of materials are measured

as a function of increasing temperature (with constant heating rate), or as a function time (with constant temperature).[106] TG-DTA can provide information about physical phenomena, such as second-order phase transitions, including vaporization, sublimation, absorption and desorption. Likewise, TG-DTA can provide information about chemical phenomena including chemisorptions, desolvation, decomposition and solid-gas reactions.

Thermal gas desorption mass spectrometry (TDMS) is the method of observing the dehydrogenation gases of the samples. During a temperature-programmed desorption, the amount of the released gas, specifically H_2 in this work, can be detected by mass spectrometry.

In this study, the mixtures were examined by Thermo gravimetry and differential thermal analysis (TG-DTA) equipment (HITACHI BRUKER TAPS3000S) combined with Thermal gas desorption mass spectrometry (TDMS, Qulee BGM-102) upon heating up to 400 °C with a heating rate of 5 °C/min. TG-DTA equipment was installed in another glove box to avoid exposing the sample to air in their measurements.

Chapter 3

Reaction Mechanism of De/hydrogenation in Li-N-H system

3.1 Background and purpose

In this study, we choose the materials of $LiNH_2$, Li_2NH and LiH as candidates to investigate from decomposition mechanism to catalytic activity in solid-solid reactions. To date, there is seldom evidence to certificate the position and state of the catalysts

among the Li-N-H materials by using TEM. We aim to clarify the reaction mechanism in nano scale by identifying the formation site of LiH and $LiNH_2$ in the dehydrogenation process. Based on the experimental results, the mechanism and catalysis of dehydrogenation are suggested.

3.2 Experimental procedures

With the purpose of clarifying the position of each solid phase, TEM (JEOL 2010 200 KV and FEI Tecnai G^2 F20 200KV) was used to observe samples. TEM samples were prepared by spreading the dry powder on a molybdenum grid in the glove box. We heated the grid for 5 min in vacuum condition to take off the deposit builder. The subsequent sample transport and operation were performed in a specially designed Ar-filled plastic bag. A heating holder of TEM was used for in-situ dehydrogenation process to observe the formation site of each solid phase.

3.3 Results and discussions

3.3.1 The formation site of LiH and LiNH2 during the de/hydrogenation process

The formation site of each solid phase after the hydrogenation process was further evidenced by direct observations. Figure 3.1 gives the TEM images and selected-area

electron diffraction (SAED) of the hydrogenated and in-situ dehydrogenated sample without catalyst. Several remarkable features are noticed from these images. First, two kinds of particles could be distinguished by different contrast, as shown in bright field image in Figure 3.1 (a). Second, the SAED pattern was composed of diffraction spots, which were identified to mainly come from LiH and $LiNH_2$, separately. Accordingly, LiH with an average size of about 100 nm formed around the surface of $LiNH_2$ after hydrogenation, as seen in the dark field image in Figure 3.1 (b) and (c). Third, after heating at 250 °C dehydrogenation, LiH reacted with $LiNH_2$ at the interface and Li_2NH fine particles formed, as shown in Figure 3.1 (d) and (e). We observed the shrinkage and disappearance of LiH particles due to the dehydrogenation reaction.

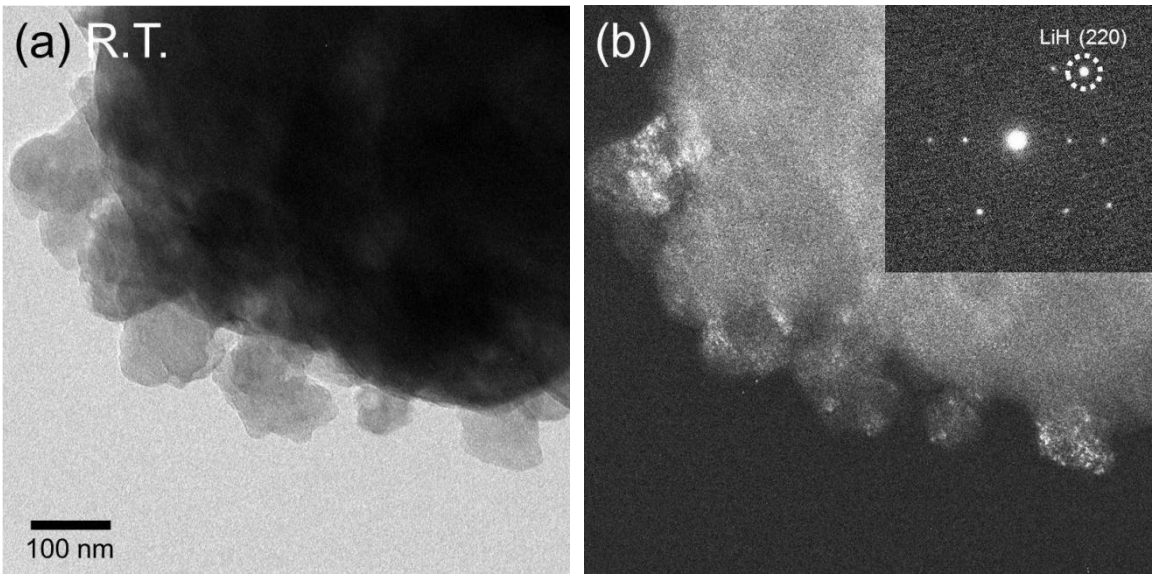

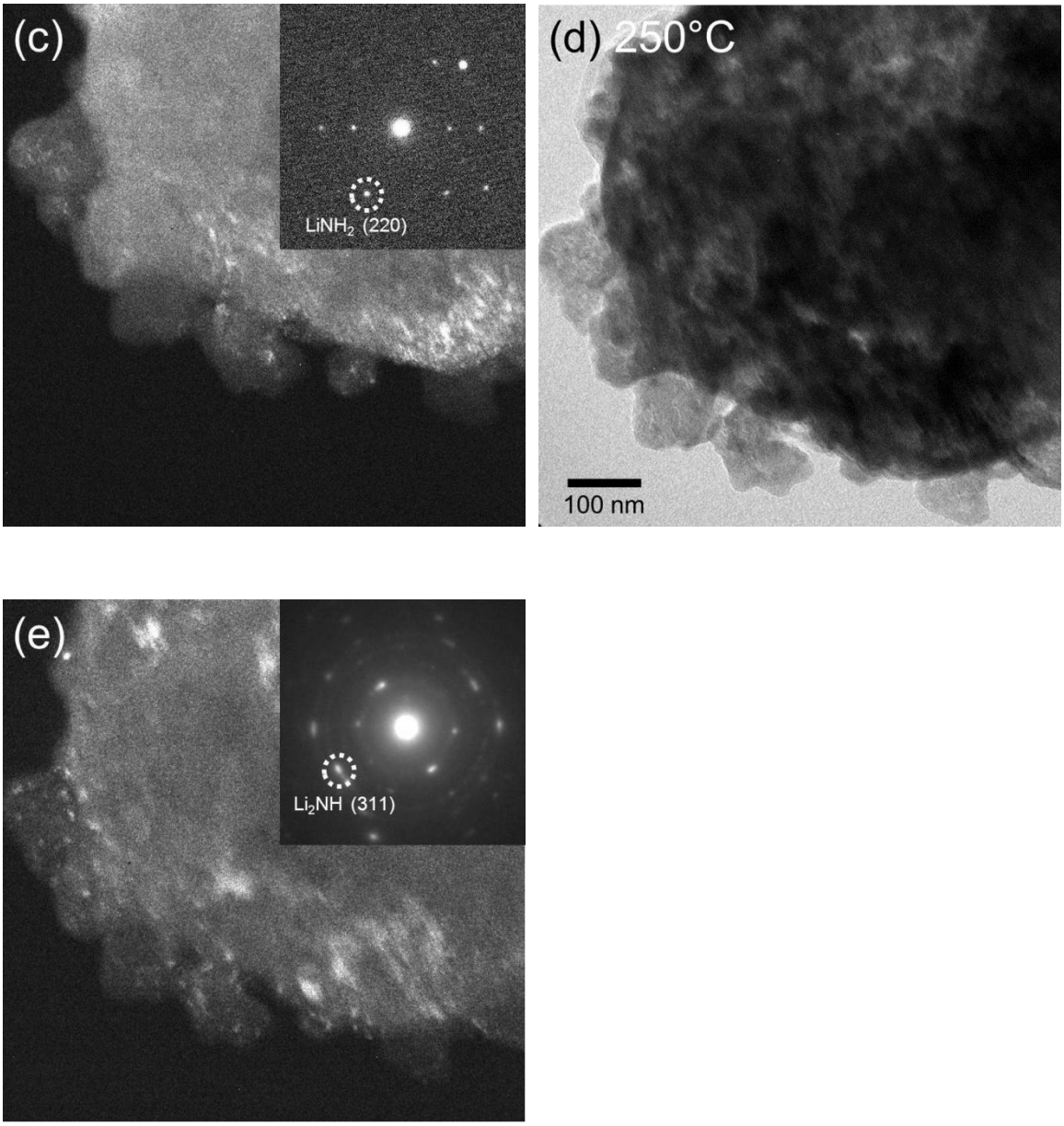

Figure 3.1. In-situ TEM observations of the $LiNH_2$ and LiH after hydrogenation: (a) bright field image; (b) dark field image and SAED of LiH; (c) dark field image and SAED of $LiNH_2$; (d) bright field image after heating; (e) dark field image and SAED of Li_2NH.

In order to clarify what kind of effect happened after doping catalyst, we observed doped sample by TEM, as shown in Figure 3.2. The SAED pattern was identified as LiH and $LiNH_2$. It should be pointed out that position of LiH and $LiNH_2$ is the same in both the sample with and without catalyst. Furthermore, LiH particle size was bigger than the sample without catalyst and in-situ dehydrogenation dramatically reacted at 200 °C. The dash white line illustrates the interface where the reaction happened (Figure 3.2 (b)). These results indicated that Li^+ ion in LiH moved to $LiNH_2$ through the interface during dehydrogenation. At the same time, H combined and released at the interface. This ionic diffusion made the dehydrogenation process to generate Li_2NH and release H_2. It is suggested that the catalyst helps the nucleation of LiH particle and enhances the dehydrogenation kinetics. From the viewpoint of the molecule structure, the skeleton of N-atoms is the same in both structure of Li_2NH and $LiNH_2$ [107]. The reaction proceeded by the migration of Li^+ ions and H. The reaction model gave a description of this system (Figure 3.2 (c)).

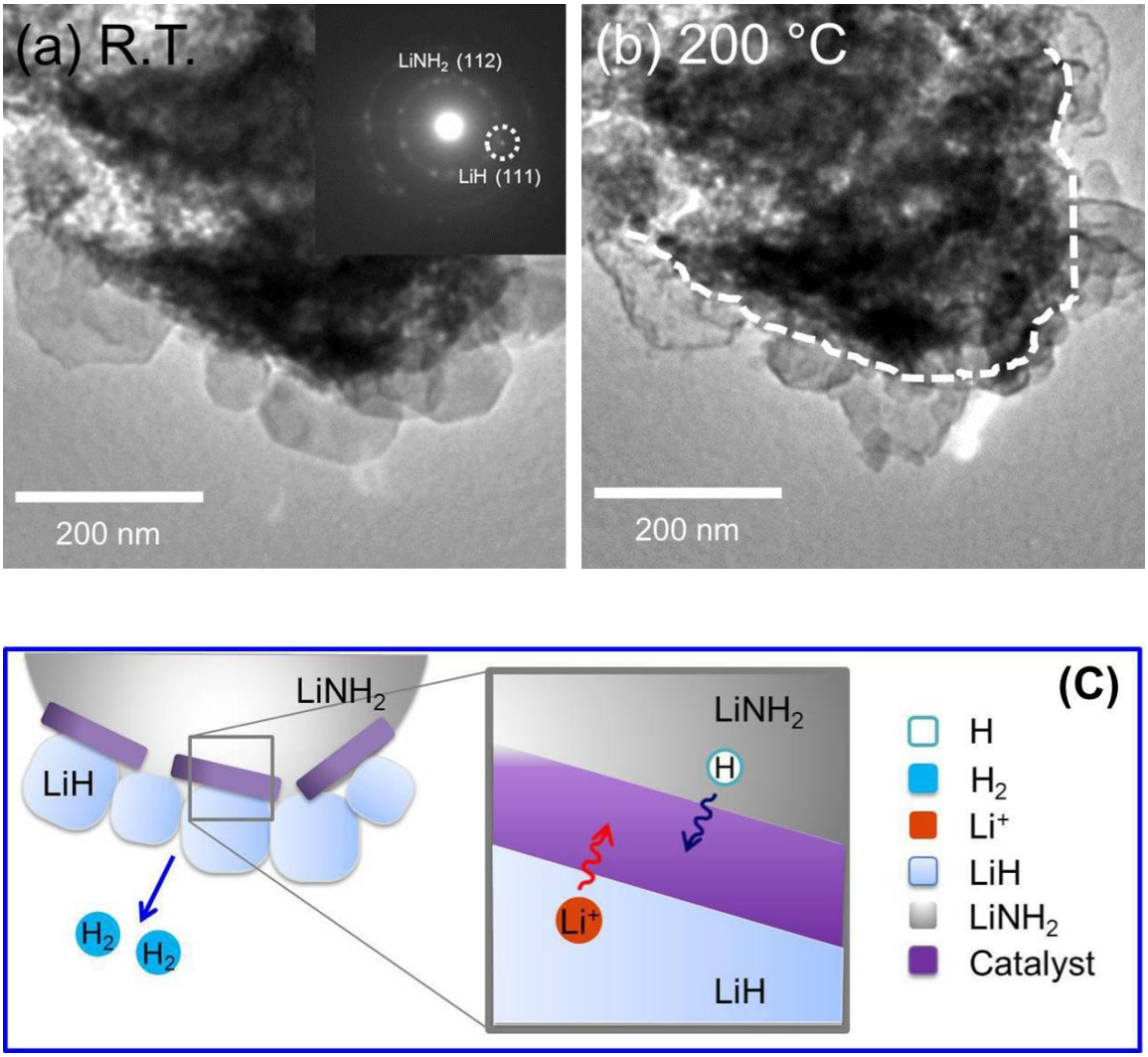

Figure 3.2. In-situ TEM observations of sample after hydrogenation with catalyst: (a) bright field image and SAED; (b) bright field image of LiNH2-Li2NH and LiH after in-situ TEM heat treatment at 200 °C. (c) Schematic reaction model.

3.3.2 The position and state of Ti compounds

Figure 3.3 shows the TEM (FEI F20) bright field image, SAED, HAADF STEM image and energy dispersive spectrometer (EDS) analysis of the hydrogenated sample with

catalyst. LiH particles formed on the surface of $LiNH_2$ particles as shown in Figure 3.3 (a). In this HAADF STEM image, the interface area between LiH and $LiNH_2$ presented bright contrast, meaning some elements with high atomic numbers were included in the area. The result of EDS from the bright area as shown in Figure 3.3 (c) provided the evidence that the particles were titanium and chlorine compound. In addition, the SAED pattern suggested that these particles were $TiCl_3$ agglomerations. These result indicated that $TiCl_3$ particles located on the interface of LiH and $LiNH_2$. LiH particles formed on the surface where was rich in catalyst.

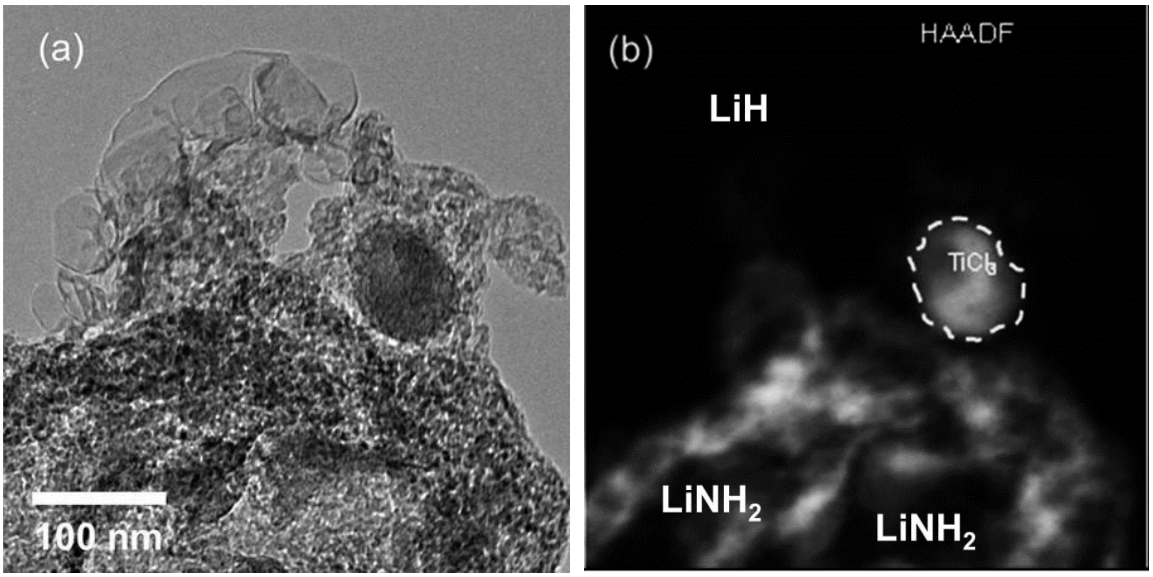

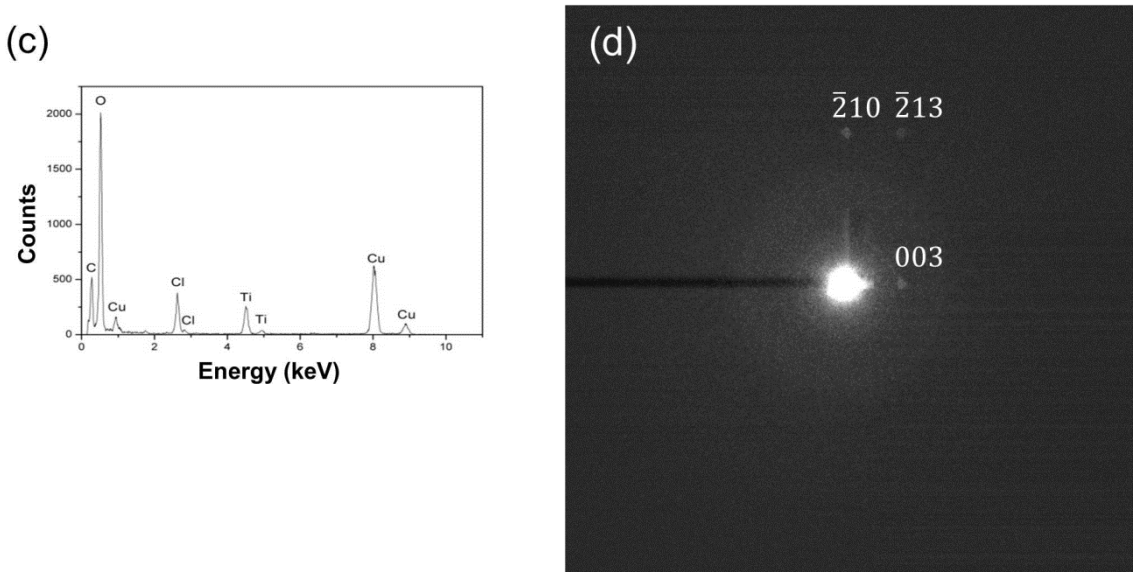

Figure 3.3. TEM images of the sample with catalyst after hydrogenation: (a) bright field image; (b) HAADF STEM image; (c) EDS of Ti and Cl compound; (d) SAED of $TiCl_3$.

Figure 3.4 shows the TEM (JEOL 2010) bright field image and SAED of the hydrogenated sample with catalyst. The particular part which found from the surface of sample was a single crystal whose size was around 200 nm, as shown in figure 4 (a). The single crystal SAED pattern was recognized as $LiTi_2O_4$. Since sample which was prepared in the glove box was carefully protected from being oxidized, the oxygen element in $LiTi_2O_4$ should mainly come from the impurities of the starting material, such as Li_2O. This result revealed that $TiCl_3$ could react with sample during the processes of high energy ball-milling in the experiment. It is also implied that $LiTi_2O_4$ could assist in the dehydrogenation process.

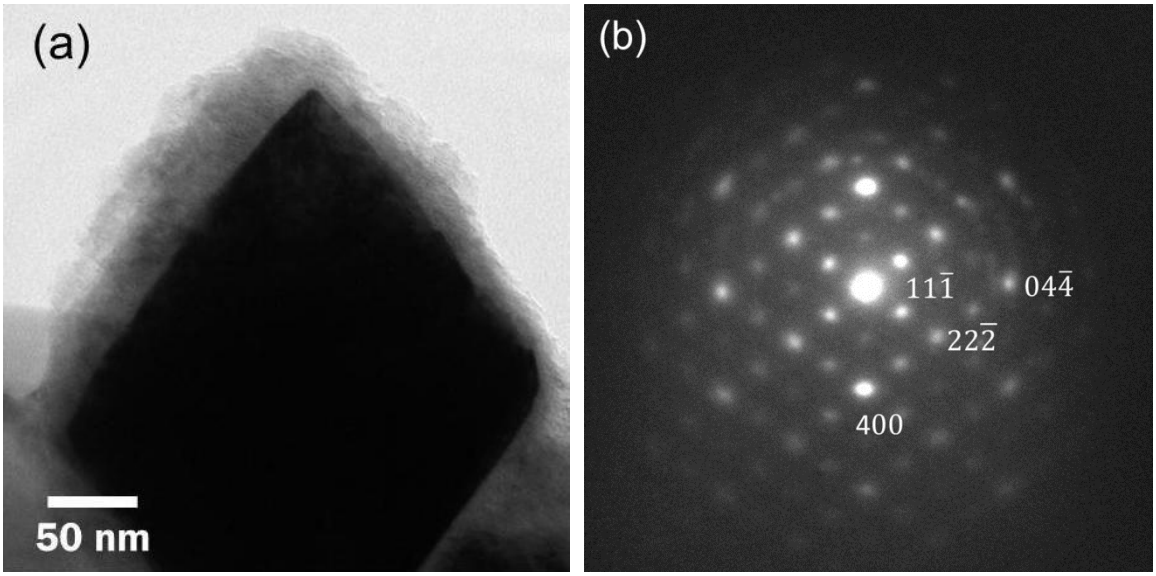

Figure 3.4. TEM images of $LiTi_2O_4$ after hydrogenation: (a) bright field image; (b) SAED of $LiTi_2O_4$.

3.3.3 Catalytic effect and decomposition mechanism model

According to the literatures [108-110], the theory was proposed to explain the catalytic effect of Ti compounds [108]. It is generally known to all that Ti like many other transition metal elements can dissociate H_2 molecule into chemisorbed hydrogen atoms. The H-H bonds break or form with an essentially lower activation energy under the assistance of Ti compounds. However, Li migration is a phenomenon of great importance in this solid-solid reaction. Li^+ ionic diffusion properties in Li_2NH and $LiNH_2$ are different. The experiment results by Li et al [111] showed that Li^+ ions presented super ionic conductivity in Li_2NH ($2.54x10^{-4}$ Scm^{-1}), while conduction of Li^+ ions was hardly detectable in $LiNH_2$ at room temperature. From these results, it is indicated that the rate

determined step is $LiNH_2$ transform to Li_2NH in dehydrogenation process. Herein, a new proposal of catalytic effect was suggested. $LiTi_2O_4$, whose high diffusion rate of Li (10^{-8} cm^2/sec) have been reported [112,113], is discovered at the surface of $LiNH_2$. Li^+ ions can diffuse in $LiTi_2O_4$ fast. It is figured that this kind of $LiTi_2O_4$ doped structure could improve Li^+ ion diffusion between $LiNH_2$ and Li_2NH, forming a kind of "lithium pump". This kind of "lithium pump" can increase the diffusion rate of Li^+, accelerating the reaction during dehydrogenation. The diagrammatic sketch is shown to describe this reaction mechanism (Figure 3.5.).

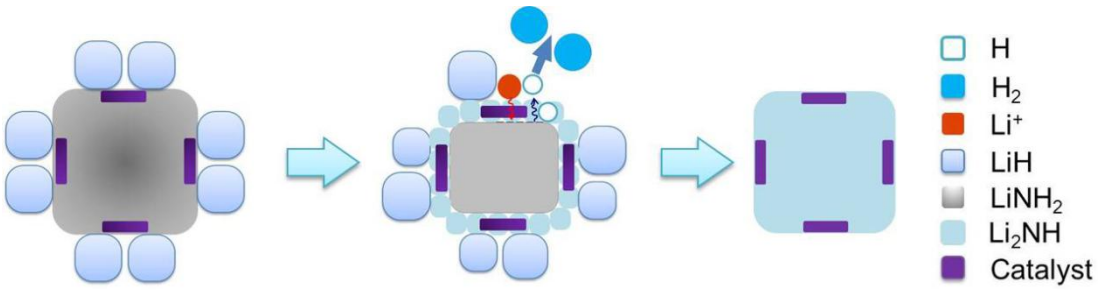

Figure 3.5. Diagrammatic sketch of the dehydrogenation reaction mechanism.

3.4 Conclusions

The decomposition mechanism of Li-N-H materials and the catalytic effect of Ti compounds in nano scale were investigated. LiH formed at the surface of $LiNH_2$ after hydrogenation. During dehydrogenation, LiH particles became smaller since it reacted with $LiNH_2$ at the interface. Ti compounds, $TiCl_3$ and $LiTi_2O_4$, located at the interface

between LiH and $LiNH_2$. The decomposition mechanism and catalysis are believed to be: (a) Li^+ ion in LiH moved to $LiNH_2$ through the interface during dehydrogenation. At the same time, H combined and released at the interface; (b) the catalyst of Ti compounds is active in the interface between LiH and $LiNH_2$. It improves Li^+ ion migrate among LiH and $LiNH_2/Li_2NH$ using less energy and improve the desorption kinetics. These results are helpful for deeper insight in hydrogen storage reactions among Li-N-H materials in nano scale.

Chapter 4

Mechanism of Catalytic Effect in Li-N-H system

4.1 Background and purpose

In the previous chapter, the results of in-situ TEM observation suggested that Li^+ ions moved from the LiH particles to the $LiNH_2$ particles through the interface during dehydrogenation.[84] Additionally, other researchers' group proposed in their report the reaction based on Li^+ migration across reactive interfaces. On the basis of these results,

it could be deduced that the kinetics of this reaction might be improved by increasing the activity of the Li^+ ions.

One attempt to enhance the hydrogen-storage properties of the Li-N-H system is to target a catalyst that would effectively increase the mobility of the Li^+ ions. In our previous study, we discovered by TEM that $LiTi_2O_4$ was in the Li-N-H sample that was doped with $TiCl_3$ as the catalyst. The catalytic Ti compounds were active at the interface between the LiH and $LiNH_2$ solid phases. Therefore, we consider $LiTi_2O_4$ as a candidate for the catalyst, but the mechanism for the catalytic effect of $TiCl_3$ remains unclear. Herein, $LiTi_2O_4$ is investigated for the Li-N-H system with the aim to enhance its hydrogen-desorption properties.

4.2 Experimental procedures

A ball-milling equipment (Fritsch P7) was used. $LiNH_2$ and LiH powders of 300 mg with 1: 1.2 molar ratio and 0.5 mol % $LiTi_2O_4$ were milled for 2 h. Furthermore, a different molar ratio of $LiTi_2O_4$ (0.5 mol %, and 2 mol %) were doped in $LiNH_2$ and LiH powders and milled for 2 h.

After the milling process, the mixtures were examined by Thermo gravimetry and differential thermal analysis (TG-DTA) equipment (HITACHI BRUKER TAPS3000S) combined with Thermal gas desorption mass spectrometry (TDMS) upon heating up to

400 °C with a heating rate of 5 °C/min. TG-DTA equipment was installed in another glove box to avoid exposing the sample to air in their measurements. Furthermore, structure properties were characterized by XRD measurement. X-ray photoelectron spectroscopy (XPS) measurement was carried out using a JPS-90MS photoelectron spectrometer with Mg Kα radiation.

4.3 Results and discussion

4.3.1 Synthesizing catalyst for the Li-N-H system

$LiTi_2O_4$ synthesized by sintering the mixture of $Li_2Ti_2O_5$ and Ti_2O_3 at 880 °C under the pressure less than 10^{-4} Pa. The powder XRD profile is given in Figure 4.1. X-ray diffraction (XRD) showed no apparent impurities in the product of the single phase of $LiTi_2O_4$. The amorphous hump in this XRD data came from the glass-substrate. The color of this single phase was black, which was consistent with the previous reports.[114]

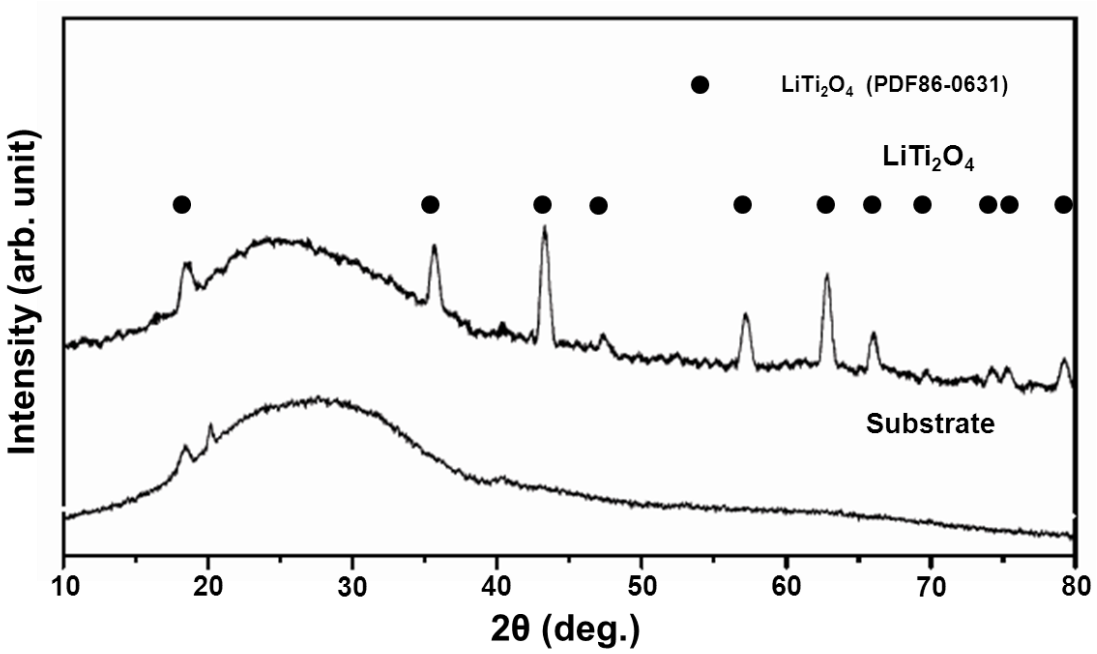

Figure 4.1. XRD pattern of the single phase of $LiTi_2O_4$.

4.3.2 Thermal desorption properties of sample with catalyst

Figure 4.2 showed the TDMS result from the composite of LiH and $LiNH_2$ with 0.5 mol % $LiTi_2O_4$. The composite of LiH and $LiNH_2$ with $LiTi_2O_4$ addition presented a sharp H_2 peak. The peak temperature was at 227 °C. No ammonia was detected by TDMS. However, the sample without $LiTi_2O_4$ released hydrogen and ammonia. The broad hydrogen desorption curves and obvious ammonia emission can be seen from 200 °C to 400 °C. Dehydrogenation profiles were obtained from both $LiNH_2$ + LiH mixture alone and with $LiTi_2O_4$.The results demonstrated clearly that there were some

effects after doping $LiTi_2O_4$(Figure 4.2). During heating, the decomposition of the $LiNH_2$ + LiH mixture was observed to start at 200 °C and complete at 400 °C. By contrast, the addition of $LiTi_2O_4$ led to full desorption within the temperature range of 150-310 °C. The total weight loss for $LiNH_2$ + LiH + 0.5 mol % $LiTi_2O_4$ was 5.7 wt. % instead of the 7.5 wt. % for $LiNH_2$ + LiH. Accordingly, a lower dehydrogenation temperature indicated that desorption properties can be improved greatly by adding $LiTi_2O_4$ as the catalyst. To the best of our knowledge, the lowest desorption temperature was achieved in the addition of $LiTi_2O_4$ to the Li-N-H system compared with other additions ($TiCl_3$, Si, BN). From the above results, it can be seen that $LiTi_2O_4$ has a catalytic effect on hydrogen desorption.

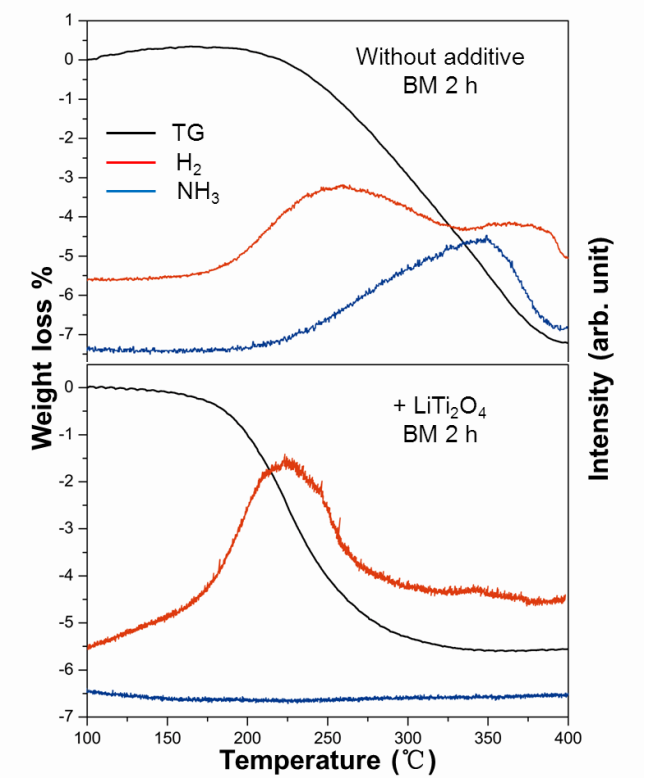

Figure 4.2. Corresponding weight loss and mass spectra of gas desorption for the dehydrogenation of $LiNH_2$ + LiH mixture milled for 2 h without any doping, and with 0.5 mol % $LiTi_2O_4$.

4.3.3 The appropriate amount of catalyst

The different amount of $LiTi_2O_4$ was doped into $LiNH_2$ + LiH mixture to elucidate the appropriate amount of $LiTi_2O_4$ in the system (Figure 4.3). Different amount of $LiTi_2O_4$ doping were attempted. According to the TG-DTA profiles, the peak-temperatures of H_2-desoprtion of 0.5 mol % $LiTi_2O_4$ doping sample was as same as the 2.0 mol %

$LiTi_2O_4$ doping sample, 227 °C. The DTA curve of 0.5 mol % $LiTi_2O_4$ doping sample was similar to this of 2.0 mol % $LiTi_2O_4$ doping sample. The experimental weight loss was 5.7 wt. % and 4.5 wt. %. A minor impurity of the starting materials, such as Li_2O, may explain the lower experimental hydrogen capacity. The reaction started at 150 °C and ended at 310°C for both samples. These results indicated no simple relationship between the catalytic effect and the amount of additive. The appropriate amount of $LiTi_2O_4$ should be 0.5 mol % considering of the more capacity of hydrogen.

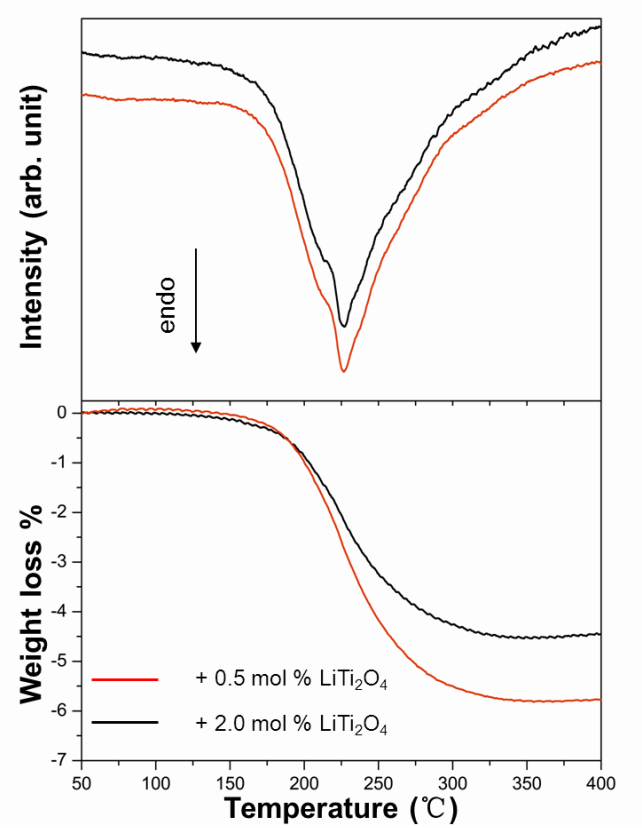

Figure 4.3. Differential thermal analysis and corresponding weight loss for the dehydrogenation of $LiNH_2$ + LiH mixture milled for 2 h with different amount of additive, 0.5 mol % $LiTi_2O_4$ and 2 mol % $LiTi_2O_4$, respectively.

4.3.4 The stability of catalyst state

The stability of $LiTi_2O_4$ is reflected by the XRD patterns in Figure 4.4. After high-energy ball milling and dehydrogenation, the structure of $LiTi_2O_4$ was as same as the single phase of the raw $LiTi_2O_4$.

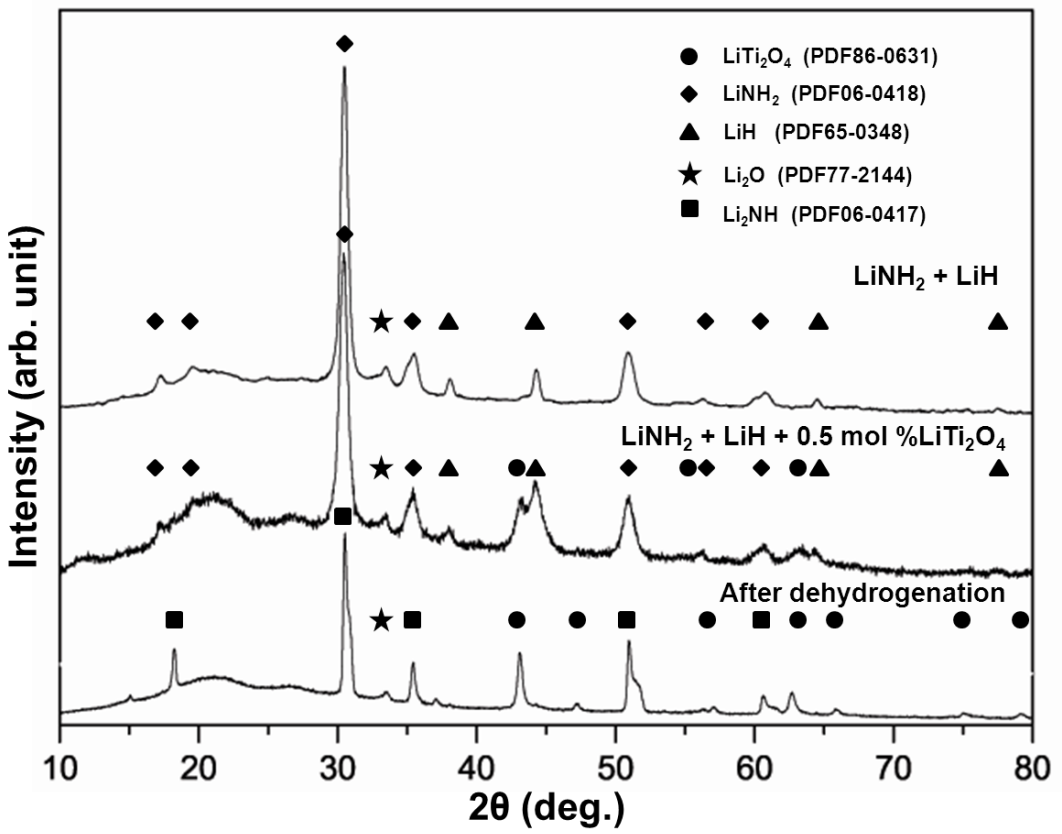

Figure 4.4. XRD patterns of the LiNH2 and LiH milled 2 h; $LiNH_2$ and LiH milled with 0.5 mol % $LiTi_2O_4$ for 2 h before TG measurement and $LiNH_2$ and LiH milled with 0.5 mol % $LiTi_2O_4$ after the TG measurement up to 400 °C.

Meanwhile, X-ray photoelectron spectroscopy (XPS) measurements were carried out for further investigation. $LiTi_2O_4$ contained with Ti (III) and Ti (IV). The titanium (Ti2p) spectra were shown in Figure 4.5. after calibration. Normally, the Ti2p region can be decomposed into two contributions corresponding to the different states of titanium in $LiTi_2O_4$. A doublet between the $2p_{3/2}$ and $2p_{1/2}$ peaks is contained in each contribution. The spectrum corresponding to the original $LiTi_2O_4$ was shown in Figure 4.5(a). Two doublets composed of two symmetric peaks were characterized, they include: (i) Ti (III) from $LiTi_2O_4$. The symmetric peaks situated at $E_b(Ti2p_{3/2})$ = 457.4 eV and $E_b(Ti2p_{1/2})$ = 463.1 eV, in agreement with the literature.[115, 116] (ii) Ti (IV) from $LiTi_2O_4$. The two symmetric peaks of the doublet have the following binding energies: $E_b(Ti2p_{3/2})$ = 458.7 eV and $E_b(Ti2p_{1/2})$ = 464.4 eV, as reported in the literature.[115-117] The spectrum of sample after high energy ball-milling and heat treatment is shown in Figure 4.5(b). Each doublet made up of two symmetric peaks after further separation. The energy binding for each doublet is as the same as the original sample. This indicated that the Ti in the cycled sample retains essentially in $LiTi_2O_4$ state. The phase of $LiTi_2O_4$ kept itself stability after high energy ball-milling and dehydrogenation.

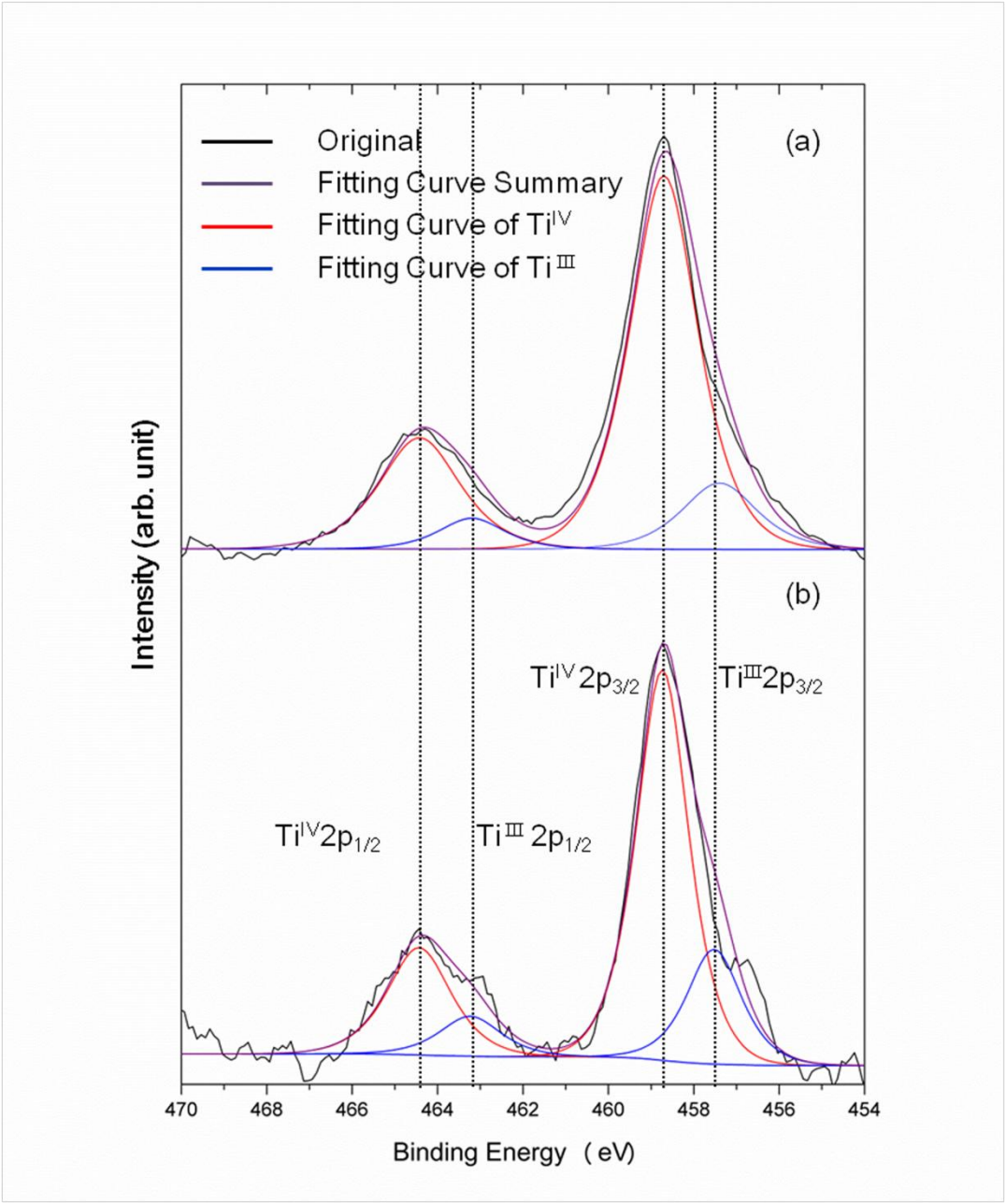

Figure 4.5. XPS spectra of the Ti2p region; (a) the original $LiTi_2O_4$ and (b) sample with 0.5 mol % $LiTi_2O_4$ after high energy ball-milling and dehydrogenation.

It can be concluded that $LiTi_2O_4$ can effective catalyse the reaction between LiH and $LiNH_2$ on hydrogen desorption, based on the above results. As far as the catalytic mechanism of a Ti compound in Li-N-H system is concerned, some investigations have been performed. According to the opinion of our previous TEM results, the characteristic state of the Ti compound, which reveals the catalytic effect, is generated by nanocontact between sample and the Ti compound in the mechanical milling process, forming $LiTi_2O_4$ compound that might have a catalytic effect on the Li-N-H system. In the present studies, $LiTi_2O_4$ has been experimentally proved to have a catalytic effect on the Li-N-H system. Basically, $LiTi_2O_4$ is a kind of superconductive material with a high diffusion rate of Li^+ which reported to be 10^{-8} cm^2/sec.[118] In order to clarify the catalytic mechanism, the crystal structure of $LiTi_2O_4$ has been concerned. Li^+ ions insert into $LiTi_2O_4$ to form $Li_2Ti_2O_4$, which can release Li^+ ions at ambient temperature.[119] Li^+ ions effortlessly diffuse in $LiTi_2O_4$ to form an intermediate phase $LiTi_2O_4$ (Figure 4.6(a)). According to the characteristic of structure, $LiTi_2O_4$ can absorb Li^+ ions from LiH, forming an intermediate $Li_2Ti_2O_4$ compound that can desorb the excess Li^+ ions to $LiNH_2$ during the dehydrogenation. This process forms a kind of "lithium pump" which can improve the mobility of Li^+ ions (Figure 4.6(b)). Meanwhile, the improvement of desorption kinetics could lead to the consumption of $LiNH_2$ and therefore the ammonia emission at high temperature could be restricted.

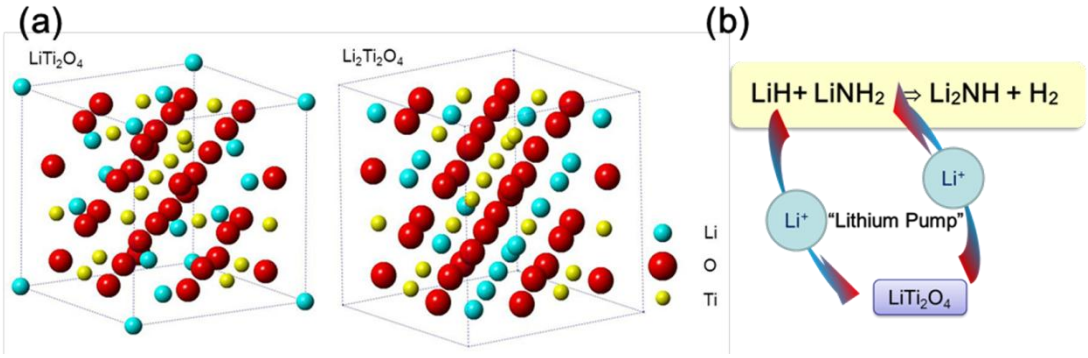

Figure 4.6. (a) Crystal structure of $LiTi_2O_4$ as well as $Li_2Ti_2O_4$ which is obtained by lithiation of the cubic $LiTi_2O_4$ phase. The lithium is completely displaced from the tetrahedral sites and fills the octahedral sites, while the titanium and oxygen positions are unchanged; (b) proposed catalytic-reaction model.

4.4 Conclusions

In summary, catalytic effects on the dehydrogenation properties of the Li-N-H system with $LiTi_2O_4$ additive were investigated. The appropriate amount and stability of $LiTi_2O_4$ on the system were confirmed by the results of TG-DTA-TDMS, XRD and XPS. During dehydrogenation, a storage capacity of 5.7 wt. % was obtained under moderate temperature. A sharp peak of hydrogen desorption occurred at 227 °C. $LiTi_2O_4$ is stable after high energy ball-milling and dehydrogenation which is reflected by the XRD patterns and XPS spectrums. The appropriate amount of additive is 0.5 mol % in the sample. The catalytic effect of $LiTi_2O_4$ probably results from the increasing of the

Li^+ ions mobility between LiH and $LiNH_2$ solid phases. The results presented here are the first to appear in the literature. It is hoped that they are helpful for achieving deeper insight into metal oxide nanoparticles catalyzed solid-solid reaction for hydrogen storage.

Chapter 5

Effect of lithium ion conduction on hydrogen desorption in Li-N-H system

5.1 Background and purpose

In the previous chapter, the catalytic effect of $LiTi_2O_4$ probably results from the increasing of the Li^+ ions mobility between LiH and $LiNH_2$ solid phases. In this chapter,

the relationship between lithium ions mobility and hydrogen desorption properties was investigated according to the alternation current (AC) impedance results.

Complex hydrides with the $(NH_2)^-$ anion are generally expressed as $M(NH_2)_n$ (n: valence of metal M), which presents ionic bonding between the M^{n+} cation and the $(NH_2)^-$ anion. Recently these materials have been researched actively as advanced hydrogen storage materials due to their high gravimetric and volumetric hydrogen densities [16, 50, 57, 94, 120 and 121]. Moreover, some of the researchers have reported that one of the complex hydrides, $LiNH_2$, expresses another chemical property, that is, lithium ionic conductivity [122-125].

The study of lithium ionic conductivity is significantly important for two sides. On one hand, it may potentially be applied to hydrogen fuel cell to improve the slow desorption kinetics and undesirable by-product gases (such as ammonia). On the other hand, it would be widely used to solid electrolytes to progress safety and energy-density related issues of lithium-ion batteries [124].

Oxide-electrolyte-materials with a special structure, such as spinels, perovskites, and fluorites, have been investigated actively due to the character of mobile interstitial ions and/or vacancies. Considering of the solid-state-reaction of complex hydrides, the mobile species of cations or anions also play an important role in the improvement of kinetics. Therefore, it is of reasonable interest to draw essence from the well-established oxide-electrolyte-systems, and provide the structural characters of these faster ionic

materials to the complex hydrides systems in order to accelerate the reaction kinetics.

5.2 Experimental procedures

The electrical conductivity was measured by ac complex impedance method by a Solartron SI-1260 impedance analyzer in a frequency range from 1 Hz to 10 MHz under the control of a PC. The sample disks (8 mm in diameter and ca. 1.5 mm in thickness) formed by pressing the powdered material were sandwiched between lithium-metal electrode and set in a 2-electrode cell in the glove box filled with purified argon. The cell was placed in a thermostatic oil bath in order to control the temperature. Temperature ranges for the measurement were from RT to above and below reaction temperatures for $LiNH_2$ and LiH mixture. The observed impedance data were analyzed as a conventional method for evaluating the electrical conductivity from the diameter of a single arc observed on the impedance plot.

5.3 Results and discussion

In order to investigate the relationship between the catalytic effects and the ionic mobility, the electrical conductivities of samples were measured by the ac impedance. It has been confirmed that the plot obtained using a lithium electrode exhibited only the semicircle, which is represented by a parallel combination of resistance and capacitance.

Herein, one plots which obtained at 383 K were shown in Figure 2(a). Their diameters decreased with increasing temperature. It would be certificated that the increased conductivity is due to the $LiNH_2$ and LiH mixtures, not the metallic $LiTi_2O_4$. As shown in Figure 2(b), the conductivity of $LiNH_2$ and LiH with catalyst was 3.93 x 10^{-6} S/cm at 423 K, which was two times higher than the sample without catalyst after same time ball-milling. The conductivity monotonically increased upon heating. Moreover, even though ball-milling time had effect on lithium ionic conductivity, when the sample was ball-milling at same time, the lithium ionic conductivities with 0.5 mol % $LiTi_2O_4$ were higher than the sample without addition.

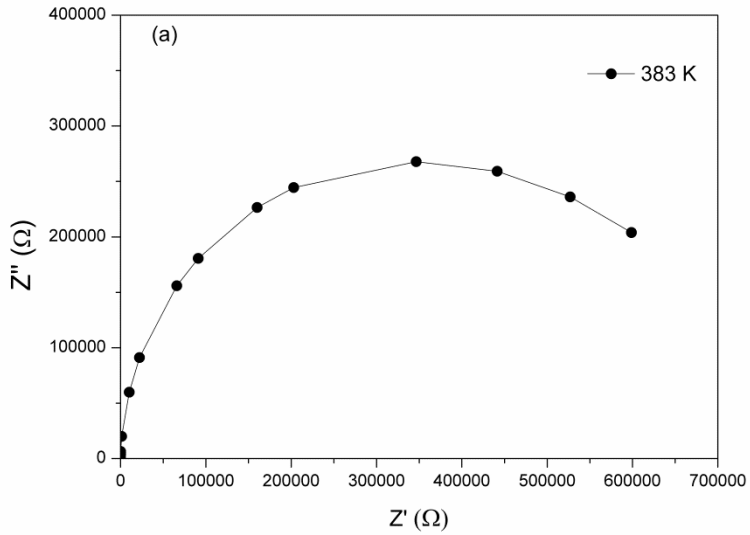

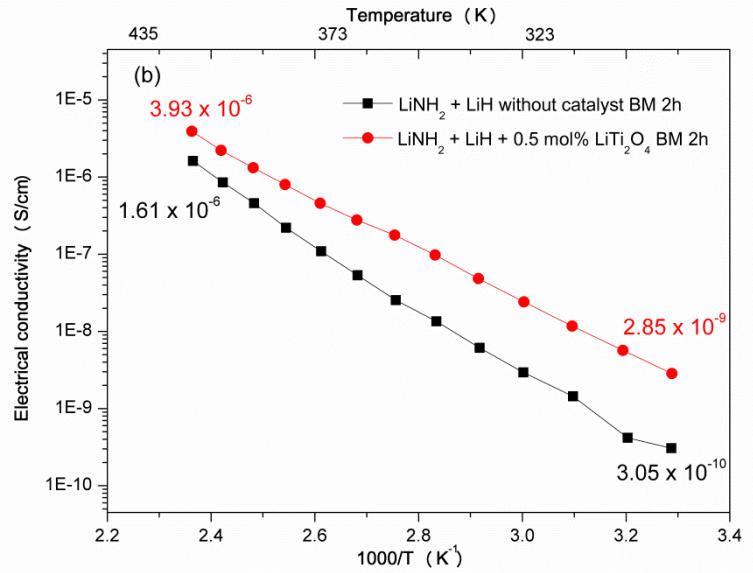

Figure 2. Electrical properties of samples with/without catalyst measured from RT to 423 K. (a) Typical impedance plots obtained using a lithium electrode at 383 K; (b) Arrhenius plots of the electrical conductivities for $LiNH_2$ and LiH mixtures.

In the previous studies [126], it was usually assumed that the temperature dependence of the ionic conductivity can be expressed by an Arrhenius equation;

$$\sigma = A/T\exp(-E/kT)$$

where σ is the ionic conductivity, T is the absolute temperature, k is the Boltzmann constant, A is the pre-exponential factor, and E is the activation energy for conductivity. When ln(σT) is plotted against 1/T, a straight line can be expected with slope –E/k and

an intercept on the ln (σT) axis of ln(A). According to the results from figure 2(b), the temperature-dependent activation energy for conductivity of sample without and with catalyst can be deduced, 0.843 eV and 0.695 eV, respectively (Table 1). It can be seen that E decreases after adding catalyst.

Furthermore, The activation energy of desorption (E_a) was estimated by Kissinger method[127] through measuring the TDMS data at different heating rates, 6 K/ min, 10 K/ min, 14 K/ min, and 18 K/ min, separately. It is according to the following equation;

$$\ln(\beta/T_p^2) = -E_a/RT_p + \ln(k_0R/E_a),$$

where β is the heating rate, T_p is the peak temperatures of desorption, R is the gas constant and k_0 is the frequency factore. If plotting $\ln(\beta/T_p^2)$ as the function of the inverse of T_p straight lines can be obtained, namely the Kissinger plot. From the slope of the straight lines Ea for the sample without and with catalyst was 90.6 kJ/mol H_2 and74.9 kJ/mol H_2, respectively (as shown in Table 1). It can be seen that E_a also decreases after doping catalyst. It is indicated that after doping catalyst, the reaction kinetics is improved due to the lithium ionic mobility increasing. It is clear that the increased conduction results in a lower hydrogen desorption temperature and an activation energy that is about 17% lower than the un-catalyzed sample.

Table 1 Correlation between Ea and E for samples without and with catalyst

Sample	Ea (activation energy of desorption, kJ/mol)	E (activation energy of lithium conductivity, eV)
w/o catalyst	90.6	0.843
w catalyst	74.9	0.695

These results suggest that, with the aid of catalyst, the reaction kinetics can be enhanced, due to the increasing mobility of cations such as Li^+ in compounds with special structure of catalyst. Herein, the details are given to explain the reaction mechanism and the catalytic effect on the solid-state reaction between $LiNH_2$ and LiH. For example, materials with fluorite structures are famous for their high conductivity.[128] Compared with the fast ionic fluorites, $LiNH_2$ forms a similarly antifluorite structure, where the position of cations and anions are reversed. Therefore, it is cations that are unstable and Li^+ are possible to migrate among different sites.[10, 129] These results have been observed in the structure studies of $LiNH_2$/Li_2NH which showed immigration of Li^+ at high temperatures during dehydrogenation.[95, 107] Additionally, our previous work indicated that the reaction mechanism based on Li^+ migration across reactive interfaces between LiH and $LiNH_2$.[84]

In the present studies, $LiTi_2O_4$ has been experimentally proved to accelerate the

lithium ionic mobility. The catalytic mechanism might be related to the crystal structure of $LiTi_2O_4$. $LiTi_2O_4$ has a spinel-structures, where Li^+ ions could go through into/out $LiTi_2O_4$ without high energy barriers at ambient temperature. Because of these characteristics of crystal structure, $LiTi_2O_4$ has a high diffusion rate of Li^+ which is reported to be 10^{-8} cm^2/sec.[118-120] All of these characters could help enhance the Li^+ ions mobility in the Li-N-H system.

5.4 Conclusions

We have reported the discovery of the relationship between the catalytic effects and the lithium ionic mobility. The conductivity of $LiNH_2$ and LiH mixtures with catalyst is nearly 1.5 times higher than the sample without catalyst. The catalytic effects of $LiTi_2O_4$ probably results from enhancing the mobility of the Li^+ ions between the LiH and $LiNH_2$ solid phases. We note that the structure characters of $LiTi_2O_4$ could improve the Li^+ ionic conductivity which is beneficial to enhance the reaction kinetics. It is hoped that Li-N-H system could be used not only in hydrogen storage but also could be applied in the lithium-ion battery materials.

Chapter 6

Conclusions and prospects

6.1 Overview

In this thesis, the reaction mechanism, as well as the catalytic effect was investigated with the purpose of Li-N-H system for hydrogen storage. The solid-state reaction mechanism, de/hydrogenation properties, mechanism of the catalytic effect, as well as the relationship between lithium ionic conduction and desorption properties in the system were studied on the basis of a series of experiments. The results and conclusions

were summarized in the following.

6.2 Solid-state reaction mechanism in Li-N-H system

The materials of $LiNH_2$, Li_2NH and LiH as candidates were investigated from decomposition mechanism to catalytic activity in solid-solid reactions.

1) According to the TEM observations, LiH formed at the surface of $LiNH_2$ after hydrogenation;

2) During dehydrogenation, LiH particles became smaller since it reacted with $LiNH_2$. Ti compounds, $TiCl_3$ and $LiTi_2O_4$, located between LiH and $LiNH_2$ particles;

3) The dehydrogenation mechanism is believed to be: Li^+ ion in LiH moved to $LiNH_2$ through the interface during dehydrogenation. At the same time, H combined and released at the interface;

4) The catalytic effect is summarized: the catalyst of Ti compounds is active in the interface between LiH and $LiNH_2$. It improves Li^+ ion migrate among LiH and $LiNH_2$/Li_2NH using less energy and improve the desorption kinetics.

6.3 Catalytic mechanism in Li-N-H system

Catalytic effects on the desorption properties of Li-N-H system with $LiTi_2O_4$ additive were studied. The appropriate amount and stability of $LiTi_2O_4$ in the system were confirmed by the results of TG-DTA-MASS, XRD and XPS.

1) A storage capacity of 5.7 wt.% was obtained under moderate temperature. A sharp peak of hydrogen desorption occurred at 227 °C;

2) $LiTi_2O_4$ is stable after high-energy ball-milling and heat treatment which is suitable used as catalyst in Li-N-H system. The appropriate amount of additive is 0.5 mol%;

3) The catalytic effect of $LiTi_2O_4$ probably results from the increasing of the Li^+ ions mobility between LiH and $LiNH_2$ solid phases.

6.4 Relationship between the catalytic effects and lithium ionic mobility

The conductivity of $LiNH_2$ and LiH mixtures with catalyst was detected by AC impedance. After comparing with the activation energy of reaction and the activation energy of lithium ionic conduction, it is clear that the increased conduction results in lower hydrogen desorption temperature and activation energy.

1) The conductivity of $LiNH_2$ and LiH mixtures with catalyst is nearly 1.5 times higher than the sample without catalyst;

2) The activation energy of reaction of sample with catalyst is about 1.2 times lower than the un-catalyzed mixture;

3) The catalytic effects of $LiTi_2O_4$ probably results from enhancing the mobility of the Li^+ ions between LiH and $LiNH_2$ solid phases.

6.5 Prospects of future work

Recently, scientists have continually working ahead in the new field of energy, especially in hydrogen-energy and lithium-ion batteries. Liquid-hydrogen cars developed by Toyota Corporation has been come into the market, and gradually become the popular vehicles on the market (http://www.toyota.com/fuelcell/). At the same time, the large-capacity of lithium-ion battery pack developed by Panasonic has been successfully used in the Tesla Motors in the United States (http://www.teslamotors.com/jp/about/press/releases/panasonic-presents-first-electric-vehicle-battery-tesla). These efforts alleviated energy problems caused by the depletion of fossil fuels. However, these two kinds of energy are used separately in both areas. The single energy composition and application systems could not meet the consumer demands for car mileage. Meanwhile, the related security problems have been plaguing

both the car manufacturers and consumers.

Herein, in order to solve these problems, it should be considering of finding a series of materials which not only could absorb H_2, but also could be used as lithium-ion solid-electrolyte in lithium-ion battery. A high efficiency and safety mode can be established. A dual-mode system link hydrogen-energy system to lithium-ion battery. To realize this idea it need to develop a series of materials to bind the hydrogen storage material with the lithium-ion solid electrolyte materials, such as $LiNH_2$, $LiAlH_4$, and $LiBH_4$.

References

1. Basic Research Needs for Electrical Energy Storage—a report of the Basic Energy Sciences Workshop on Electrical Energy Storage. April 2-4, 2007. U.S. Department of Energy Report, July 2007.
2. J. K. Dowson, Nature, 1974, 249, 724.
3. M. S. Dresselhaus, I. L. Thomas, Nature, 2001, 414, 332.
4. L. Schlapbach, A, Züttel, Nature, 2001, 414, 353.
5. J. Graetz, Chem. Soc. Rev., 2009, 38, 73.
6. http://en.wikipedia.org/wiki/Energy_density.
7. http://www.hydrogen.energy.gov/.
8. R. von Helmolt and U. Eberle, J. Power Sources, 2007, 165, 833.
9. http://www1.eere.energy.gov/hydrogenandfuelcells.
10. H. Wu, ChemPhysChem, 2008, 9, 2157.
11. http://www.hfpeurope.org/.
12. W. Grochala, P. P. Edwards, Chem. Rev., 2004, 104, 1238.
13. A. W. C. van den Berg, C. O. Areán, Chem. Commun., 2008, 668.
14. G. Sandrock, J. Alloys Compd., 1999, 295, 877.
15. M. Dornheim, S. Doppiu, G. Barkhordarian, U. Boesenberg, T. Klassen, O. Gutfleisch, R. Bormann, Scr. Mater., 2007, 56, 841.

16. S. Orimo, Y. Nakamori, J. R. Eliseo, A. Züttel, C. M. Jensen, Chem. Rev., 2007, 107, 4111.

17. P. Chen, M. Zhu, Mater. Today, 2008, 11, 36.

18. P. Wang, X. D. Kang, Dalton Trans., 2008, 5400.

19. F. Schüth, B. Bogdanović, M. Felderhoff, Chem. Commun. 2004, 2249.

20. H. W. Langmi, G. S. McGrady, Coord. Chem. Rev., 2007, 251, 925.

21. J. Graetz, Chem. Sov. Rev., 2009, 38, 73.

22. D. H. Gregory, J. Mater. Chem., 2008, 18, 2321.

23. D. H. Gregory, Chem. Rec., 2008, 8, 229.

24. D. H. Gregory, in Solid State Hydrogen Storage-Materials and Chemistry, ed. G. Waker, Woodhead Publishing, Cambridge, 2008, pp. 450-477.

25. http://en.wikipedia.org/wiki/Category:Metal_hydrides

26. B. Sakintuna, F. Lamari-Darkrim, M. Hirscher, Int. J. Hydrogen Energy, 2007, 32, 1121.

27. D. Grant, in Solid State Hydrogen Storage-Materials and Chemistry, ed. G. Waker, Woodhead Publishing, Cambridge, 2008, pp. 357-380.

28. K. C. Hoffman, J. J. Reilly, F. J. Salzano, C. H. Waide, R. H. Wiswall, W. E. Winsche, Int. J. Hydrogen Energy, 1976, 1, 133.

29. R. Schulz, J. Huot, G. Liang, S. Boily, G. Lalande, M. C. Denis, J. P. Dodelet, Mater. Sci. Eng. A, 1999, 267, 240.

30. J. Huot, M. L. Tremblay, R. Schulz, J. Alloys Compd., 2003, 356-357, 603.

31. T. Vegge, L. S. Hedegaard-Jensen, J. Bonde, T. R. Munter, J. K. Norskov, J. Alloys Compd., 2005, 386, 1.

32. W. Oelerich, T. Klaassen, R. Bormann, Adv, Eng. Mater., 2001, 3, 487.

33. V. M. Skripnyuk, E. Rabkin, Y. Estrin, R. Lapovok, Acta Mater., 2004, 52, 405.

34. N. Hanada, T. Ichikawa, H. Fujii, J. Phys. Chem. B, 2005, 109, 7188.

35. G. Barkhordarian, T. Klassen, R. Bormann, J. Alloys Compd., 2004, 364, 242.

36. G. Barkhordarian, T. Klassen, R. Bormann, Scr. Mater., 2003, 49, 213.

37. V. V. Bht, A. Rougier, L. Aymard, X. Darok, G. Nazri, J. M. Tarascon, J. Power Sources, 2006, 159, 107.

38. J. J. Vajo, G. L. Olson, Scr. Mater., 2007, 56, 829.

39. H. Wu, CHemPhysChem, 2008, 9, 2157.

40. S. A. Shevlin, Z. X. Guo, Chem. Soc. Rev., 2009, 38, 211.

41. M. Mamatha, B. Bogdanovic, M. Felderhoff, A. Pommerin, W. Schmidt, F. Schuth and C. Weidenthaler, J. Alloys Compd., 2006, 407, 78.

42. B. C. Hauback, Z. Kristallogr., 2008, 223, 636.

43. B. Bogdanovic, M. Schwickardi, J. Alloys Compd., 1997, 1, 253.

44. S. S. Srinivasan, H. W, Brinks, B. C. Hauback, D. Sun, C. M. Jensen, J. Alloys Compd., 2004, 377, 283.

45. X. B. Yu, Z. Wu, Q. R. Chen, Z. L. Li, B. C. Weng, T. S. Huang, Appl. Phys. Lett. 2007, 90, 034106.

46. J. Yang, A. Sudik, C. Wolverton, J. Phys. Chem. C, 2007, 111(51), 19134.

47. J. J. Vajo, S. L. Skeith, J. Phys. Chem. B, 2005, 109(9), 3719.

48. H. Wu, W. Zhou, K. Wang, T. J. Udovic, J. J. Rush, T. Yildirim, L. A. Bendersky, A. F. Gross, S.

L. V. Atta, J. J. Vajo, F. E. Pinkerton, M. S. Meyer, Nanotechnology, 2009, 20, 204002.

49. Z. Z. Fang, L. P. Ma, X. D. Kang, P. J. Wang, P. Wang, H. M. Cheng, Appl. Phys. Lett., 2009, 94, 044104.
50. P. Chen, Z. Xiong, J. Z. Luo, J. Y. Lin, K. L. Tan, Nature, 2002, 420, 302.
51. T. Ichikawa, S. Isobe, N. Hanada, H. Fujii, J. Alloys Compd., 2004, 365, 271.
52. T. Ichikawa, N. Hanada, S. Isobe, H. Leng, H. Fujii, J. Phys. Chem. B, 2004, 108, 7887.
53. S. Isobe, T. Ichikawa, N. Hanada, H. Leng, M. Fichtner, O. Kircher, H. Fujii, J. Alloys Compd., 2005, 404, 439.
54. S. Isobe, T. Ichikawa, Y. Kojima, H. Fujii, J. Alloys Compd., 2007, 446, 360.
55. H. Y. Leng, T. Ichikawa, S. Hino, H. Fujii, J. Alloys Compd., 2008, 463, 462.
56. W. F. Luo, J. Alloys Compd., 2004, 381, 284.
57. W. Luo, S. Sickafoose, J. Alloys Compd., 2006, 407, 274.
58. F. H. Stephens, V. Pons, R. T. Baker, Dalton Trans., 2007, 2613.
59. B. Peng, J. Chen, Energy Environ. Sci., 2008, 1, 479.
60. T. B. Marder, Angew. Chem., Int. Ed., 2007, 46, 8116.
61. P. Wang, X. D. Kang, Dalton Trans., 2008, 5400.
62. A. Gutowska, L. Y. Li, Y. S. Shin, C. M. M. Wang, X. H. S. Li, J. C. Linehan, R. S. Smith, B. D. Kay, B. Schmid, W. Shaw, M. Gutowski, T. Autrey, Angew. Chem., Int. Ed., 2005, 44, 3578.
63. Y. S. Chen, J. L. Fulton, J. C. Linehan, T. Autrey, J. Am. Chem. Soc., 2005, 127, 3254.
64. V. Sit, R. A. Geanangel, W. W. Wendlandt, Thermochim. Acta, 1987, 113, 379.
65. S. G. Shore, R. W. Parry, J. Am. Chem. Soc., 1955, 77, 6084.

66. W. T. Klooster, T. F. Koetzle, P. E. M. Siegbahn, T. B. Richardson, R. H. Crabtree, J. Am. Chem. Soc., 1999, 121, 6337.

67. Z. Xiong, C. K. Yong, G. Wu, P. Chen, W. Shaw, A. Karkamkar, T. Autrey, M. O. Jones, S. R. Johnson, P. P. Edwards, W. I. F. David, Nat. Mater., 2008, 7, 138.

68. A. W. C. van den Berg, C. O. Arean, Chem. Commun., 2008, 668.

69. M. Uhlemann, O. Gutfleisch, A. Leonhardt, A. Graff, C. Taschner, J. Fink, Appl. Phys. Lett., 2002, 80, 2985.

70. H. Schimmel, G. Nijkamp, G. Kearley, A. Rivera, K. de Jong, F. Mulder, Mater. Sci. Eng., B, 2004, 108, 124.

71. B. Panella, M. Hirscher, S. Roth, Carbon, 2005, 43, 2209.

72. J. Sangster, A. D. Pelton in Phase Diagrams of Binary Hydrogen Alloys; (Ed.: F. D. Manchester), ASM International, Materials Park, 2000, pp.74.

73. J. J. Vajo, F. Mertens, C. C. Ahn, R. C. Bowman, Jr., B. J. Fultz, J. Phys. Chem. B 2004, 108, 13977.

74. R. C. Bowman, Jr., S. J. Hwang, C. C. Ahn, J. J. Vajo, Mater. Res. Soc. Symp. Proc. 2005, 837, 3.6.1.

75. H. Wu, W. Zhou, T. J. Udovic, J. J. Rush, T. Yildirim, Phys. Rev. B 2006, 74, 224101.

76. H. Wu, W. Zhou, T. J. Udovic, J. J. Rush, Chem. Mater. 2007, 19, 329.

77. H. Wu, W. Zhou, T. J. Udovic, J. J. Rush, T. Yildirim, Chem. Phys. Lett. 2008, 460, 432.

78. E. Wieberg, R. Bauer, M. Schmidt, R. Z. Uson, Naturforsch, 1951, 6b, 393.

79. B. Bogdanović, M. Schwickardi, J. Alloys Compd. 1997, 253, 1.

80. W. Oelerich, T. Klassen, R. Borman, J. Alloys Compd. 2001, 315, 237.

81. G. Barkhordarian, T. Klassen, R. Bormann, J. Phys. Chem. B 2006, 110, 11020.

82. N. Hanada, T. Ichikawa, S. Isobe, T. Nakagawa, K. Tokoyoda, T. Honma, H. Fujii, Y. Kojima, J. Phys. Chem. C, 2009, 113, 13450.

83. T. Ichikawa, N. Hanada, S. Isobe, H. Y. Leng, H. Fujii, J. Alloys Compd. 2005, 404-406, 435.

84. T. Zhang, S. Isobe, Y. Wang, N. Hashimoto, S. Ohnuki. RSC Adv. 2013, 3, 6311.

85. M. Kajitani, M. Matsuda, A. Hoshikawa, S. Harjo, T. Kamiyama, T. Ishigaki, F. Izumi, M. Miyake, Chem. Mater. 2005, 17, 4235.

86. H. Hayashi, H. Inaba, M. Matsuyama, N. G. Lan, M. Dokiya, H. Tagawa, Solid State Ionics 1999, 122, 1.

87. P. R. Slater, J. T. S. Irvine, T. Ishihara, Y. Takita, J. Solid State Chem. 1998, 139, 135.

88. K. Ikeda, Y. Kogure, Y. Nakamori, S. Orimo, Scripta Mater. 2005, 53, 319.

89. K. Ikeda, S. Kato, Y. shinzato, N. Okuda, Y. Nakamori, A. Kitano, H. Yukawa, M. Morinaga, S. Orimo, J. Alloy Compd. 2007, 446-447, 162.

90. T. W. D. Farley, W. Hayes, S. Hull, M. T. Hutching, M. Vrtis, J. Phys. Condens. Matter 1991, 3, 4761.

91. M. Hayoun, M. Meyer, A. Denieport, Acta Mater. 2005, 53, 2867.

92. H. Wu, W. Zhou, T. J. Udovic, J. J. Rush, T. Yildirim, Chem. Mater. 2008, 20, 2335.

93. S. Nayebossadri, K. F. Aguey-Zinsou, *Phys. Chem. Chem. Phys.*, 2011, 13, 17683.

94. K. F. Aguey-Zinsou, J. Yao, Z.X. Guo, J. Phys. Chem. B, 2007, 111, 12531.

95. W.I.F. David, M.O. Jones, D.H. Gregory, C.M. Jewell, S.R. Johnson, A. Walton, P.P. Edwards, J.

Am. Chem. Soc. 2007, 129, 1594.

96. P. Kichambare, N. Kijima, S. Honma, S. Ebisu, S. Nagata, J. Phys. Chem. Solids 1996, 57, 1615.
97. F. Xu, Y. C. Liao, M. J. Wang, C. T. Wu, K. F. Chiu, M. K. Wu, J. Low Temp. Phys. 2003, 131, 569.
98. M. Rygula, S. Kemmler-Sack, T. Nissel, R. P. Hubener, Ann. Phys. (Leipzig) 1993, 2, 685.
99. D. W. Murphy, M. Greenblatt, S. M. Zahurak, R. J. Cava, J. V. Waszczak, G. W. Hull, Jr. and R. S. Hutton, Rev. Chim. Miner. 1982, 19, 441.
100. E. Moshopoulou, PhD. Dissertation University Joseph Fourier-Grenoble I, Grenoble-France, March 1995.
101. P. Scherrer, Göttinger Nachrichten Gesell. , 1918, 2, 98.
102. A. Patterson, Phys. Rev. 1939, 56, 978.
103. http://en.wikipedia.org/wiki/Scherrer_equation
104. H. Yao, S. Isobe, Y. Wang, N. Hashimoto, S. Ohnuki, J. Electron Microsc. Tech., 2011, 60(6), 375.
105. http://en.wikipedia.org/wiki/X-ray_photoelectron_spectroscopy
106. http://en.wikipedia.org/wiki/Thermogravimetric_analysis
107. M. P. Balogh, C. Y. Jones, J. F. Herbst, L. G. Hector Jr and M. Kundrat, J. Alloys Compd., 2006, 420, 326.
108. T. J. Frankcombe, Chem. Rev., 2012, 112, 2164.
109. E. Ivanov, I. Konstanchuk, A. Stepanov, V. Boldyrev, J. Less Common Met., 1987, 131, 25.
110. B. Bogdanović, U. Eberle, M. Felderhoff, F. Schüth, Scr. Mater., 2007, 56, 813.

111. W. Li, G. Wu, Z. Xiong, Y. P. Feng, P. Chen, Phys. Chem. Chem. Phys., 2012, 14, 1596.

112. O. W. Johnson, Phys. Rev. A, 1964, 136, 284.

113. J. Bhattacharya, A. VanderVen, Phys. Rev. B: Condens. Matter Mater. Phys., 2010, 81, 104304.

114. L. H. Yang, C. Dong, H. H. Song, J. Guo, G. C. Fu, Chin. Phys. Lett. 2005, 22, 243.

115. B. Siemensmever, J. W. Schultze, Surf. Interface Anal. 1990, 16, 309.

116. J. Pouilleau, D. Devilliers, H. Groult, J. Mater. Sci. 1997, 32, 5645.

117. C. D. Wagner, W. M. Riggs, L. E. Davis, J. F. Moulders, G. E. Mullenberg, in 'Handbook of X-ray photoelectron spectroscopy', edited by G. E. Mullenberg (Perkin-Elmer Corporation, Eden Prairie, MN, 1979).

118. O. W. Johnson, Phys. Rev. A 1964, 136, 284.

119. R. J. Cava, D. W. Murphy, S. Zahurak, J. Solid State Chem. 1984, 53, 64.

120. T. Zhang, S. Isobe, Y. Wang, N. Hashimoto, S. Ohnuki, ChemCatChem, 2014, 6, 724.

121. T. Zhang, S. Isobe, Y. Wang, H. Oka, H. Hashimoto, S. Ohnuki, J. Mater. Chem. A, 2014, 2, 4361.

122. P. A. Anderson, P. A. Chater, D. R. Hewett, P. R. Slater, Faraday Discuss., 2011, 151, 271.

123. M. Matsuo, T. Sato, Y. Miura, H. Oguchi, Y. Zhou, H. Maekawa, H. Takamura, S. Orimo, Chem. Mater. 2010, 22, 2702.

124. M. Matsuo, A. Remhof, P. Martelli, R. Caputo, M. Ernst, Y. Miura, T. Sato, H. Oguchi, H. Maekawa, H. Takamura, A. Borgschilte, A. Züttel, S. Orimo, J. Am. Chem. Soc. 2009, 131, 16389.

125. N. Ohta, K. Takada, L. Zhang, R. Ma, M. Osada, T. Sasaki, Adv. Mater. 2006, 18, 2226.

126. J. A. Kilner, B. C. H. Steele, in ‘Nonstoichimetric Oxides’, edited by O. T. Sorensen. New York: Academic Press, 1981, 233.

127. H. E. Kissinger, Anal Chem, 1957, pp. 1702-1706.

128. M. Conradi, B. Corey, R. Bowman, R. Jr., Zidan, A private communication.

129. G. C. Allen, P. A. Tempest, J. W. Tyler, Nature, 1982, 295, 48.

Acknowledgements

I would like to express my gratitude to all those who helped me during the writing of this thesis.

My deepest gratitude goes first and foremost to Professor Somei Ohnuki and Professor Shigehito Isobe, for their constant encouragement and guidance. They have walked me through all the stages of the writing of this thesis. Without their consistent and illuminating instruction, this thesis could not have reached its present form. I am grateful to Professor Naoyuki Hashimoto for his comments and proofreading. To Professor Shigeharu Ukai and Professor Tomohiro Akiyama, my examiners who provided constructive feedback and encouraging, I would like to express my grateful thanks to you thoughtful and detailed comments during my doctoral course, and the contribute you have imparted for the progress of this work. Then I would like to thank Professor Shin-ichi Orimo and Professor Motoaki Matsuo, not only for their great help on my research, but also for their encouragement that urged me on to work hard.

Second, I would like to express my heartfelt gratitude to Dr. Yongming Wang, who helped me during my stay in this laboratory and how to use TEM. Special thanks to Dr. Wang for his continuous help during these years and enable me to develop an intimate understanding of this subject. He has given me a lot help to broaden my horizon in this research area.

High tribute shall be paid to Ms. Kaori Kobayashi for making my stay an enjoyable

one and for her warmly welcome and providing a wonderful family atmosphere in our lab.

I wish to thank all of students in the Lab of Advanced Materials. The senior students, Chuanzhi Yu, Chuanxin Liu, Hao Yao, Tao Ma, Siwei Chen, Shuai Wang, Takanobu Wakasugi, Hiroshi Oka, and Miki Dohkoshi, thanks for teaching me how to use different experimental equipment. The same grade students, Ayaka Umeda, Yuki Nakagawa, Bin Zhou, Tomoki Kubota, Hiroto Hatashi, Bumsu Park, and Junya Tanimoto, thanks for discussion together in different research area. The junior students, Ryo Yamagami, Hirotaka Honma, Yudai Ikarashi, Shotaro Chiba, Tomonori Kimura, Kohei Tadaki, and Xiaoyu Zhao, thanks for the concern of my stay in Hokkaido. I wish to express my thanks to all my friends for their friendship and the nice moments we spend together.

Finally, I am deeply indebted to my parents and my fiancée Xiaoran Doris QIN for their continuous support and encouragement. I owe my sincere gratitude to my mother country, China, who gave me her help during the difficult time of the thesis.